A FINITE-ELEMENT MODEL OF THE MIDDLE EAR OF THE MOUSTACHED BAT

McGill University,
Montréal, Québec

November 2000

A thesis submitted to the Faculty of Graduate Studies and Research
in partial fulfilment of the requirements for the degree of

Master of Engineering

Prospero:
"*Dost thou hear?*"

Miranda:
"*Your tale, Sir, would cure deafness.*"

Shakespeare, The Tempest, Act 1, Scene 2.

ABSTRACT

Recently smooth-muscle tissue has been observed in the annular ligament of the moustached bat, *Pteronotus parnellii*. In order to lead to improved understanding of the function of this highly developed smooth-muscle system surrounding the tympanic membrane, a finite-element model was developed.

The complex geometry of the middle ear was defined using both magnetic-resonance microscopy and histological data. Contributions were made to the locally written software which was used for image segmentation and finite-element mesh generation.

The action of the smooth-muscle fibres is modelled by applying a radial load to the model of the tympanic membrane. The radial load is represented by placing load vectors tangential to the model of the tympanic membrane.

Simulations were carried out in order to investigate convergence, sensitivity to tympanic-membrane shape, and to evaluate the effects of pressure and radial loads.

RÉSUMÉ

Dernièrement, des chercheurs ont noté la présence de fibres musculaires lisses dans le ligament annulaire de la chauve-souris à moustache (*Pteronotus parnellii*). Afin de mieux comprendre la fonction de ce système de fibres musculaires lisses qui entoure la membrane tympanique, nous avons élaboré un modèle d'éléments finis.

La géométrie complexe de l'oreille moyenne a été établie au moyen de la microscopie à résonance magnétique et de données histologiques. Des suggestions ont été faites pour améliorer le logiciel élaboré à l'interne qui a été utilisé pour segmenter les images et générer des maillages d'éléments finis.

Le mouvement des fibres musculaires lisses a été simulé par l'application d'une charge radiale au modèle de la membrane tympanique; la charge radiale étant représentée par des vecteurs de charge positionnés tangentiellement par rapport au modèle.

Des simulations ont été menées afin d'examiner la convergence, la sensibilité à la forme de la membrane tympanique, et différents effets résultant de la pression et des charges radiales.

TABLE OF CONTENTS

1

CHAPTER 1 ..... **1**

INTRODUCTION **1**

CHAPTER 2 ..... **4**

AUDITORY SYTEM **4**

2.1 GENERIC STRUCTURE 4

2.2 IMPEDANCE TRANSFORMATION 6

CHAPTER 3 ..... **8**

THE BAT **8**

3.1 INTRODUCTION 8

3.2 THE MOUSTACHED BAT PTERONOTUS PARNELLII 8

3.2.1 Introduction *8*

3.2.2 Echolocation *9*

3.2.3 Muscle tissue *10*

3.3 ANATOMY OF THE BAT MIDDLE EAR 10

3.3.1 Tympanic membrane *10*

3.3.2 Ossicular chain *11*

3.3.3 Muscles *16*

CHAPTER 4 ..... **21**

FINITE-ELEMENT METHOD **21**

4.1 INTRODUCTION 21

4.2 RITZ-RAYLEIGH PROCEDURE 22

4.3 SINGLE-ELEMENT ANALYSIS 23

4.4 MULTIPLE-ELEMENT ANALYSIS 25

4.5 DYNAMIC MODELS 26

CHAPTER 5 27

METHODS 27

5.1 INTRODUCTION 27

5.2 MRM 27

5.2.1 Introduction *27*

5.2.2 MRM data *28*

5.3 HISTOLOGY 30

5.3.1 Introduction *30*

5.3.2 Data *31*

5.4 SEGMENTATION 33

5.4.1 Introduction *33*

5.4.2 Edge-based segmentation techniques *33*

5.4.3 Open and closed contours *34*

5.4.4 Segmentation programmes *36*

5.4.5 Tr3 header *38*

5.4.6 Segmented MRM data *44*

5.5 MESH GENERATION 46

5.5.1 Mesh *46*

5.5.2 Bandwidth *48*

5.5.3 Node placement *48*

CHAPTER 6 ..... **50**

THE FINITE-ELEMENT MODEL **50**

6.1 INTRODUCTION 50

6.2 TYMPANIC MEMBRANE 52

6.3 ANNULAR LIGAMENT 54

6.4 OSSICULAR CHAIN 55

6.4.1 Malleus & incus *56*

6.4.2 Stapes *56*

6.5 MATERIAL BEHAVIOUR 57
6.6 ACOUSTICAL INPUT 57
6.7 OVERALL MESH 57

CHAPTER 7 ..... **59**

RESULTS **59**

7.1 INTRODUCTION 59
7.2 CONVERGENCE TEST 59
7.3 STATIC DISPLACEMENTS 62
7.4 EFFECTS OF TYMPANIC-MEMBRANE SHAPE 64
7.5 EFFECTS OF SMOOTH MUSCLE IN ANNULAR LIGAMENT 65
7.6 UNCLAMPED MANUBRIUM 67

CHAPTER 8 ..... **68**

CONCLUSION AND FUTURE WORK **68**

8.1 SUMMARY 68
8.2 CONCLUSION 69
8.3 FUTURE WORK 70

REFERENCES **72**

APPENDIX 1 ..... **79**

TR3 HEADER **79**

LIST OF FIGURES

Figure	Page
2.1 Human auditory system.	4
3.1 *Pteronotus parnellii* Moustached bat.	8
3.2 Medial view of the tympanic membrane, malleus, and tensor tympani muscle.	10
3.3 A lateral view of the ossicular chain.	11
3.4 A medial view of part of the ossicular chain of the *Nyctalus noctula.*	12
3.5 Average and standard deviations of the measurements of the ossicles.	13
3.6 Medial view of the malleus of the *Myotis myotis.*	14
3.7 The incus of the *Rhinolophus euryale.*	14
3.8 The stapes of the *Rhinolophus ferrumequinum.*	15
3.9 A schematic illustration of the different structures of a muscle.	16
3.10 The tensor tympani connected to the malleus.	18
3.11 The stapedius muscle connected to the stapes.	18
3.12 A close-up of the radial shaped annular ligament and tympanic membrane.	19
4.1 A simple two-element system with two triangular elements.	25
5.1 Slice number 110 from set 16963.	29
5.2 A digitised part of a histological slide of the moustached bat.	31
5.3 Enlargement of histology slide with folded structures.	32
5.4 Schematic illustration of open and closed contours.	35
5.5 Part of MRM image of subject 12148. Example of single-layer segmentation.	35
5.6 Schematic illustration of a structure.	41
5.7 MRM image and corresponding segmented areas.	44
5.8 Segmentation and reduced segmentation.	44
5.9 Part of the segmentation of slice 114 of subject number 12148.	45
5.10 Graph of the total computational solution time versus the number of nodes.	47
5.11 MRM image and histology slice showing the direction of the load vectors.	49

6.1 A VRML representation of the complete model. 50
6.2 MRM Slice 156 with distortions due to the preparation of the specimen. 52
6.3 Side views of the tympanic membrane and manubrium. 53
6.4 Triangulation of part of the model. 54
6.5 Medial view of the combined malleus and incus, and tympanic membrane. 56
6.6 Medial view of the stapes with four springs attached to the footplate. 56
6.7 Triangulation of the model. 58
7.1 Minimum and maximum displacements along x axis 61
7.2 Graph of min and max displacements along z axis and maximum displacement of the magnitude 61
7.3 Visualisation of the displacement patterns along the different axes and the displacement magnitude with the manubrium and the annular ligament clamped 63
7.4 Visualisation of the displacement patterns along the x axis with the manubrium and the annular ligament clamped. 64
7.5 Three visualisations of the displacement patterns along the x axis for an applied radial load; an applied radial load & applied pressure; and only an applied pressure. 66
7.6 A visualisation of the displacement patterns along the x axis with the manubrium unclamped, and the annular ligament clamped. 67

ACKNOWLEDGEMENTS

I could not have made it without all the people around me, people who supported me in many ways. I wish to thank them all. In particular I wish to thank my supervisor, Professor W. Robert J. Funnell, for his support and patience; my parents Bert and Truus van Wijhe for their everlasting support and understanding; my late grandaunt and granduncle Annie Allard-van Wijhe and Mick Allard, for teaching me that there is more in life and making it all possible; my girlfriend Jennifer, for her support and love throughout my study; my colleague Salim Abou Khalil, for his input and cheerful presence; and Drs. O.W. Henson Jr. and M. Henson for their input.

This work was supported in part by the Canadian Institutes of Health Research, the Natural Sciences and Engineering Research Council (Canada), and VSB Fonds (The Netherlands). We thank The Center for In Vivo Microscopy (CIVM), Duke University for providing the MRM data.

Chapter 1

INTRODUCTION

The human hearing system is one of the body's most fascinating sensory organs. It is capable of actively transforming acoustical signals into an electrical output; of determining minimal changes in stimulus intensity; and of an enormous amount of amplitude compression whereby the hearing system can distinguish incoming signals varying by several orders of magnitude, from a needle dropping on a table to an explosion.

To get a better understanding of the mechanical behaviour and properties of the middle ear, a particular part of the hearing system, models of this structure are developed. The middle ears of both humans and other mammals are used for modelling. It is common in hearing research that species other than humans are the subject of experimentation to develop and evaluate models for both normal and pathological aspects of the hearing system. This is because the anatomy of terrestrial mammals is comparable to that of humans, and because experimental data needed for validation of the models are more readily available from non-human subjects.

Several techniques are employed in modelling the mechanics of the middle ear. The first mathematical models of the tympanic membrane and middle ear were lumped-parameter models in the form of mechano-acoustical circuits or their equivalent electrical circuits. These kinds of models were built by Onchi (1961), Zwislocki (1962), Shaw & Stinson (1981), and many others.

In lumped-parameter models the mechanical or acoustical behaviour of the anatomical structure is represented by a combination of three idealised circuit elements: a point mass, an ideal spring and an ideal damper. The parameter values for the model are obtained by trying to fit the behaviour of all or part of the model to experimental results.

Another lumped-parameter approach uses two-port "black boxes," which are characterised by 2x2 matrices. The elements of these matrices are also obtained empirically.

Lumped-parameter approaches produce models which are able to replicate specified experimental data. The main disadvantage of these models is the relatively loose ties between the parameters and the physiological or anatomical data independent of the behaviour being modelled. For example, a change in behaviour, such as changes in vibration patterns due to muscle contractions or a shift of stimulus frequency, will change the estimated mass completely.

The mechanical behaviour of the structure can also be studied with the use of the finite-element method. The structure is divided into elements with a finite size. The geometries of these elements are simple enough to permit analytical intra-element solutions of the differential equations. The model is defined in terms of the anatomical shape and biomechanical material properties like stiffness, damping, etc.

Funnell (1975) was the first to present the finite-element method as a tool for analysing the mechanical behaviour of the tympanic membrane of the cat and other species. Over the last few years this approach has evolved, and the newest model of the cat includes elastic suspensions of the malleus and incus, and also takes the mass and damping of the structure into account (Funnell & Laszlo, 1978; Funnell et al., 1992). More recently, finite-element models of the human middle ear (Abou et al., 2000) and of the gerbil middle ear (Funnell et al., 1999) have been presented. Several other researchers have also presented their finite-element models of the human middle ear (e.g., Beer et al., 1997; Wada, et al., 1992; Ferris et al.,1998; Lord et al., 1999)

In this thesis the modelling of the middle ear of the moustached bat (*Pteronotus parnellii rubiginosa*) is described. Particular attention is devoted to the recently observed smooth muscle fibres present in the annular ligament of the tympanic membrane. The model will contribute to the analysis of the potential effects of tonic radial tension on the mechanical behaviour of the tympanic membrane and its role in sound transmission. It may also give more insight into clinical applications like ossicular prosthesis development and impedance tympanometry. It may also contribute to some clinical applications like tympanoplasty, where a higher tension may be applied to the tympanic membrane, combining adjustable tension of the tympanic membrane, for example, with cochlear implants to obtain the most effective signal to noise ratio.

Chapter two presents a general overview of the mammalian auditory system; in Chapter Three the moustached bat will be introduced and a more detailed description of the anatomy of the bat middle ear will be given; Chapter Four presents the finite-element method; and Chapter Five will present the method of modelling. Chapter Six will give a description of the actual model and the simulation results are presented in Chapter Seven. The conclusions and future work are discussed in Chapter Eight.

Chapter 2

AUDITORY SYTEM

2.1 Generic structure

The physiology of hearing of terrestrial mammals appears qualitatively similar. This section will give an overview of the auditory system. Figure 2.1 shows an overall anatomical representation of the human auditory system.

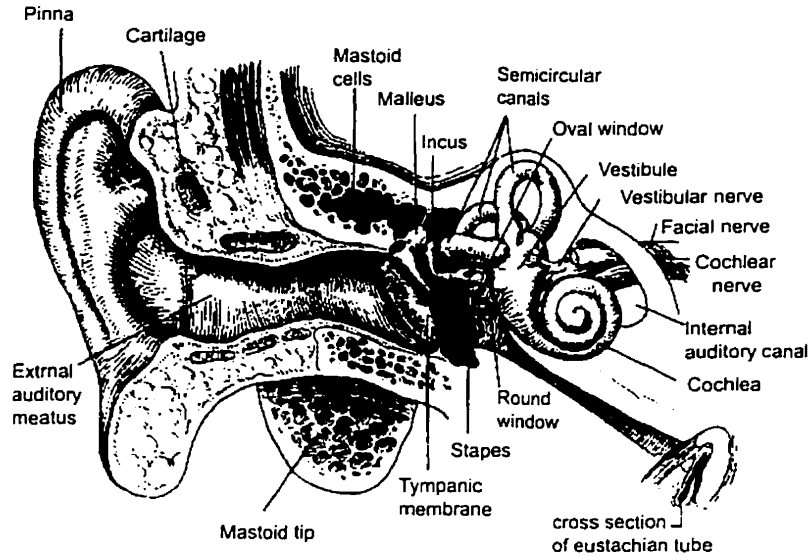

Figure 2.1

The auditory system

From: "*Auditory physiology: The Earmark of RLE Research*" by Dorothy A. Fleischer, December 1989 edition of RLE currents.

The auditory system can be partitioned into three subsystems: the external, middle, and inner ear. The external ear consists of the pinna and external auditory meatus. The pinna captures sound-pressure waves in open air and guides them into the external auditory meatus.

This is a narrow elliptically shaped channel which directs the waves towards the tympanic membrane. The tympanic membrane is made of several different layers of tissue. The membrane is connected to the bony portion of the ear canal, the tympanic ring, by means of the annular ligament.

The middle ear is an air-filled space containing the three auditory ossicles, the malleus, incus, and stapes, and two muscles: the tensor tympani and stapedius. The three ossicles form a chain, called the ossicular chain, which links the tympanic membrane to the oval window of the cochlea. The manubrium, which is part of the malleus, is connected to the tympanic membrane, and the footplate of the stapes is connected to the oval window. The muscles play a significant role in suppressing excessive movement of the chain due to high sound pressures.

The middle ear is separated from the inner ear by the oval window of the cochlea, which is part of the inner ear. The inner ear may be divided into the auditory labyrinth or cochlea, and the vestibular labyrinth. The cochlea is a snail-shaped bony canal with three fluid filled chambers winding around from base to apex. The ossicular chain transfers the sound-pressure wave to the oval window and causes the fluid within the cochlea to move. Sensory cells, located in the middle chamber, are capable of transducing the mechanical movement of the liquid into an electrical signal which is passed to the auditory cortex by the cochlear nerve.

The middle ear may be seen as an impedance matching transformer, providing a bridge between the air-borne pressure waves setting the tympanic membrane into motion and the liquid-borne travelling waves of the cochlea. The direct stimulation of the fluid in the cochlea would be ineffective due to the difference in impedance of the cochlear fluid and air. The acoustical properties of liquid and water differ in such a way that 99.9% of the sound energy at an air-water interface will be reflected and only 0.1% will be transferred to the fluid body (Wever & Lawrence, 1954). The presence of the middle ear overcomes this problem by transforming the incoming signal.

2.2 Impedance transformation

The middle ear is an impedance matching transformer of the incoming acoustic sound pressure. The impedance transformation is often described as a set of three different mechanisms: the surface area ratio between the oval window and tympanic membrane; the lever action of the ossicular chain; and the curvature of the tympanic membrane.

The difference in surface area will cause the sound wave pressure to be concentrated on a smaller area. The transformation is proportional to the ratio of the effective areas. Since the force applied to the tympanic membrane is approximately the same as the force reaching the oval window, the pressure at the oval window will be greater than that at the tympanic membrane. This can be shown with formula 2.1:

$$p = \frac{F}{A} \tag{2.1}$$

where p is the pressure applied, F is the force, and A is the surface area. By keeping F constant and changing the surface area, the applied pressure (p) will go up. This would be the case if the tympanic membrane were to vibrate as a hinged plate and the footplate of the stapes were to act as a piston. Unfortunately, neither is true. Khanna & Tonndorf (1972) showed that the behaviour of the tympanic membrane is far from that of a hinged plate, and as for the motion of stapes, recently Decraemer et al. (2000) concluded:

> *"At all frequencies the motion of the stapes has a large piston-like component but other substantial components are also present."*

The lever action of the ossicles is related to the fact that the manubrium is longer than the long process of the incus, which increases the force, while decreasing the velocity at the stapes footplate. The theory behind this mechanism has been described by Relkin (1988), for example.

It would be true if the tip of the manubrium, the umbo, was the only point of attachment, but the manubrium is connected to the tympanic membrane along its full length. In addition, the ossicles do not move as a rigid unit, which in turn influences the lever action.

The third mechanism is the so-called "curved-membrane effect" which was first proposed by Helmholtz (1869). The lever ratio is related to the curvature of the membrane. Helmholtz's hypothesis was later supported by Khanna and Tonndorf (1972). More recently, Funnell (1996) found that

> *"...certain regions of the ear drum are more effective in driving the manubrium than can be explained on the basis of their distance from the axis of rotation. This enhanced coupling depends on the curvature of the eardrum but, unlike the mechanism hypothesized by Helmholtz, requires neither tension nor anisotropy."*

Although many researchers see the three different mechanisms as distinct, research has shown that their individual input is hard to distinguish. Funnell (1996) concluded:

> *"...the effective surface area of the eardrum depends on the displacement distribution, and this and the curvature-related lever mechanism both depend on the geometry and material properties in interrelated ways."*

Chapter 3

THE BAT

3.1 Introduction

Several researchers have studied the middle ear of the taxon *Chiroptera*: the bats. The morphology was described by Hyrtle (1845), and Staněk (1933) presented highly detailed illustrations of the peripheral auditory system of several species of the suborder *Microchiroptera*. In addition, Doran (1878), Wassif (1948) and Tepaske (1964) gave precise descriptions of the ossicles. Wilson & Bruns (1983) measured the acoustic vibrations of the tympanic membrane and of the stapes in the greater horseshoe bat. This chapter presents the moustached bat and describes its ability to echolocate. Experimental data on the moustached bat are scarce and the anatomy of the different species is similar, so a generic overview of the anatomy of the middle ear of bats belonging to the order of microchiroptera follows.

3.2 The moustached bat Pteronotus parnellii

3.2.1 Introduction

The moustached bat (*Pteronotus parnellii*) can be distinguished by stiff hairs around its mouth, which give the appearance of a moustache. It has folds of skin on its lower lip, its chin is covered by wart-like bumps, and the colour of its fur is medium- to dark-brown. Its weight at maturity is approximately 10 to 14 grams and its wingspan is about 340 to 350 mm. It lives deep in the large inner chambers and passageways of caves, in colonies of approximately 5000 bats, and feeds upon insects.

Figure 3.1

Pteronotus parnellii Moustached bat, Brazil. Photo by L. H. Emmons. © Smithsonian Institution, 1997.

The moustached bat belongs to the suborder *Microchiroptera*. This type of bat makes use of echolocation to find its way in darkness, to avoid obstacles and to capture insect prey. Echolocation involves the emission of ultrasonic pulses which may have intensities as high as 120 dB SPL. Subsequent to the emission the system detects low-intensity reflections bouncing from obstacles and insect prey. The bat is able to attenuate the loud outgoing sounds and then be in a highly sensitive state to perceive faint echoes within a matter of milliseconds.

3.2.2 Echolocation

The moustached bat emits pulses in order to echolocate obstacles and to capture insect prey. There are three phases of emission: the orientation phase, the pursuit phase, and the terminal phase. The orientation phase consists of a constant frequency (CF) with initial and terminal frequency modulation (FM). The CF has a prominent second harmonic of about 60-62 kHz which drops to about 45 kHz. The fundamental and third harmonic are also significantly present (Novick and Vaisnys, 1964). The orientation pulse lasts 20 ms (CF), the search pulse lasts 22 msec, and the terminal phase (FM) lasts 1.7 msec (Novick, 1977).

The repetition rate has been measured in a laboratory environment. For the search phase the repetition rate is approximately 14 pulses/sec, at end of the approach phase it is about 20 pulses/sec, and at the end of the terminal phase of insect pursuit it is about 80–100 pulses/sec. The pulses are long (6 to 50 ms) pure tones terminated by a brief FM sweep.

The use of ultrasonic pulses for echolocation indicates that hearing must be especially acute for high frequencies. The brief duration of the bat's sonar signals indicate that the physical characteristics of echoes and the location of echo sources are determined with only very brief exposure to the stimulus.

3.2.3 Muscle tissue

The moustached bat middle ear is equipped with a set of very well developed muscles that contract and relax in synchrony with pulse emission and echo perception (Henson, 1970). The tensor tympani and stapedius muscle are striated muscles which attenuate sounds by tensing the tympanic membrane. In addition, an annular ring of radially oriented smooth muscle has recently been reported (Henson & Henson, 2000). This may provide a regulated state of tonic tension that affects the contraction and relaxation times of the striated (twitch) muscle. The smooth-muscle arrays described in the moustached bat have also been found in other species (Henson & Henson, 2001).

3.3 Anatomy of the bat middle ear

This section describes the anatomy of the bat middle ear. As mentioned above, due to the lack of available information about the middle-ear structure of the moustached bat a more generalized description of the middle ear of bats will be presented. While there is a generic form common to all mammalian hearing systems, specific characteristics of the bat's middle ear lead to some interesting anatomical differences. The next section presents the ossicles and soft tissues of the middle ear of the bat.

3.3.1 Tympanic membrane

For all terrestrial mammalian species, the tympanic membrane is elliptical to circular in shape and it attaches to the internal circumference of the tympanic bone by means of the annular ligament. The membrane has a conical shape, the deepest part of which is called the umbo. The manubrium, which is part of the malleus, is embedded in the tympanic membrane, with the spatulated tip at the umbo.

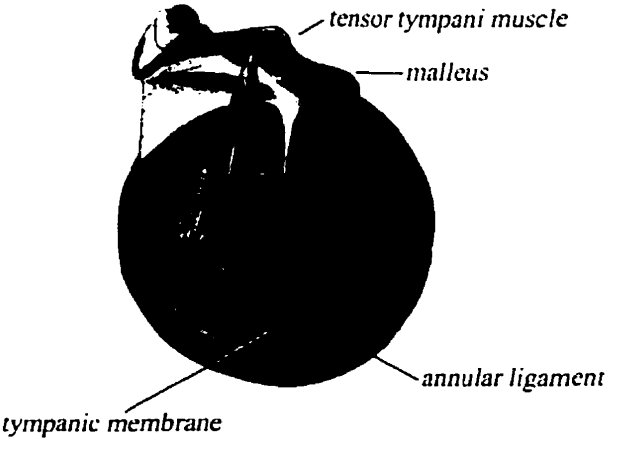

Figure 3.2
A medial view of the tympanic membrane, malleus, and tensor tympani muscle.
After Stanĕk, 1933.

The membrane consists of the pars flaccida and the pars tensa, and the latter includes most of the membrane. The fibrous centre of the membrane is a stratum made of a very thin layer of radially and circularly arranged fibres (Staněk, 1933).

The form of insertion of the annular ligament in bats was described by Bondy (1907) as different from other mammals in that it inserts over a relatively wide surface and leaves numerous gaps which are occupied by an extensive network of blood vessels. Henson & Henson (2000) recently confirmed this description, but also reported the presence of smooth muscle cells.

3.3.2 Ossicular chain

In all terrestrial mammalian species, the malleus is attached to the tympanic bone, the incus to the walls of the fossa incudis, and the stapes to the margins of the oval window. Synovial joints link the malleus and incus, and the incus and stapes. The joints of the malleus to the tympanic membrane and the stapes to the oval window are fibrous.

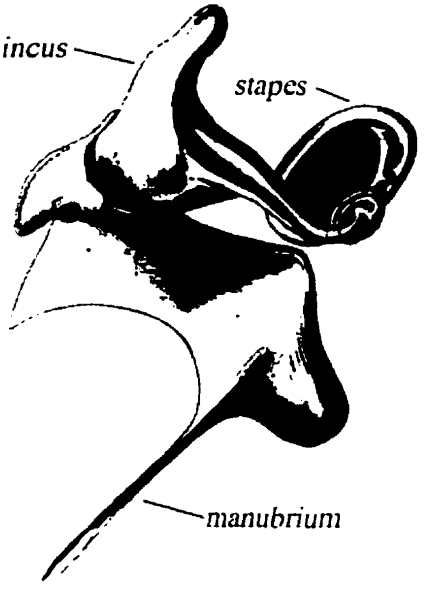

A lateral view of the ossicular chain
After Staněk, 1933.

In bats, the ossicles are smaller and more delicate than those found in other species. They have an extremely small mass, which may favour the transmission of high-frequency sounds. The malleoincudal articular surfaces are much more deeply cut than in other mammals (see Figure 3.4), suggesting a tighter coupling between the ossicles (Henson, 1970).

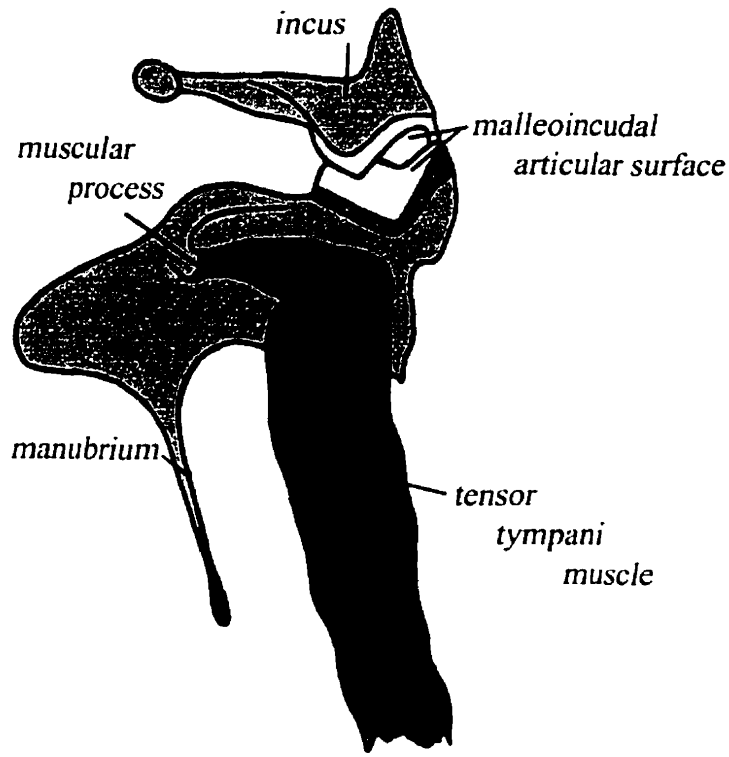

Figure 3.4
A medial view of part of the ossicular chain of
Nyctalus noctula.
After Staněk, 1933.

Staněk (1933) measured the sizes of the ossicles of 20 different species of bats. Measurements of the ossicles of the moustached bat are, unfortunately, not included in this set. To give an idea of the approximate sizes of the ossicles, the means and standard deviations of the different measurements have been calculated from the data acquired by Staněk and are shown in Figure 3.5.

	Malleus (mm)					*Incus (mm)*					*Stapes (mm)*						
	M	P	C	L	S	D	L	B	C	P	V	O	PO	P	C	COL	ANT
Mean	0.94	0.25	0.39	0.48	1.36	0.89	0.55	0.22	0.11	0.17	0.46	0.45	0.40	0.04	0.18	0.19	0.45
Standard deviation	0.22	0.10	0.12	0.13	0.33	0.23	0.15	0.07	0.03	0.04	0.13	0.08	0.11	0.05	0.04	0.04	0.12

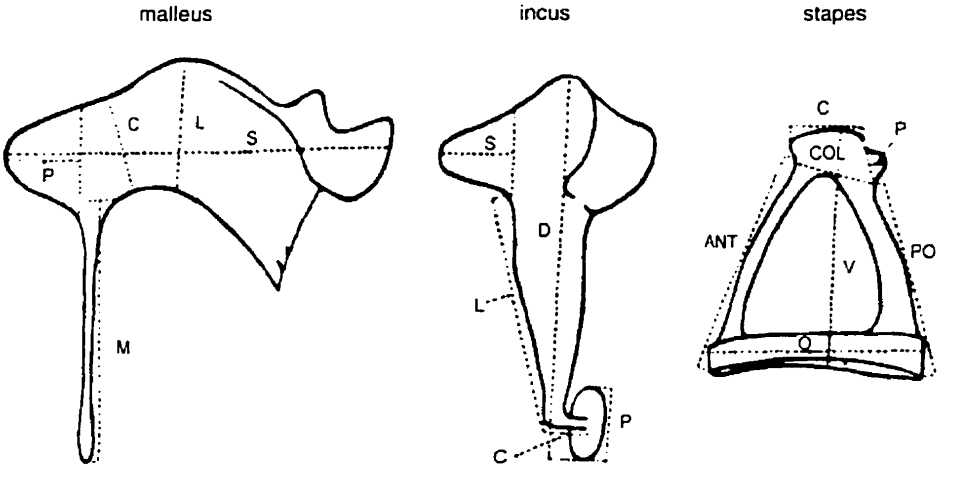

Figure 3.5

Means and standard deviations of the measurements of the ossicles of 20 different species. After Staněk, 1933

For comparison, here are some measurements of the ossicles of the human (as quoted by Wever & Lawrence, 1954).

The length from the end of manubrium to the end of lateral process of the malleus (M) is 5.8 mm (Stuhlman, 1937). For the incus, the length along the long process (D) is 7.0 mm (Stuhlman, 1937). The stapes has a mean height (V) of 3.26 mm (Bast & Anson, 1949) and the mean length of the footplate (O) of 75 ears is 2.99 mm (Bast & Anson, 1949).

Henson (1961) measured the volumes of the ossicles of *Rhinolophus ferrumequinum*. They are 0.042, 0.013 and 0.0038 mm^3, for the malleus, incus and stapes, respectively. Using a density of 1.9 g/cm^3 (Wilson, 1982) leads to estimated masses of 80, 25 and 7.2 µg. For the human these values are: 27, 32, and 3.9 mg, respectively (Wever & Laurence, 1954). For the entire ossicular chain there is a difference in mass of a factor of 624.

3.3.2.1 Malleus

The malleus consists of a manubrium, a head and a neck. The manubrium is embedded in the tympanic membrane and has a relatively large mass at the base. The head articulates with the incus, and the neck interconnects the head and manubrium. The anterior process extends anteriorly and is more sophisticated. The neck is long and sharply curved and consists of two parts: a tympanic process, and a lamina interconnecting the tympanic process with the head, neck, and manubrial base.

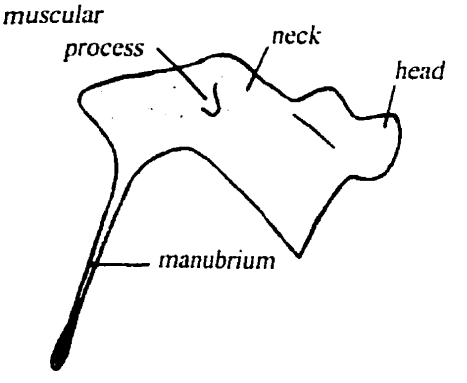

Figure 3.6
Medial view of the malleus of *Myotis myotis*.
After Stanĕk, 1933.

The malleo-tympanic articulation of the bat, which is the articulation between the upper anterior surface of the anterior limb of the tympanic bone and the tympanic process of the malleus, has been found to be an osseous ankylosis (Henson, 1961).

3.3.2.2 Incus

The incus consists of a body with an articular surface for the malleus; a long process with a lenticular process which articulates with the head of the stapes; and a short process for the posterior incudal ligament. The posterior incudal ligament is strong and well developed and consists of medial and lateral parts.

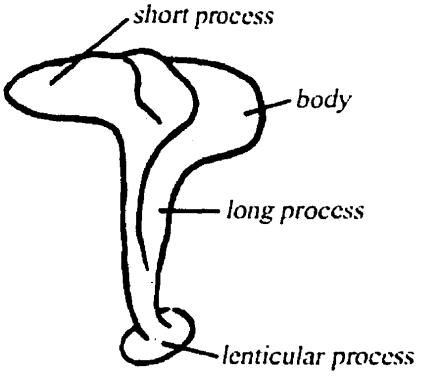

Figure 3.7
The incus of *Mrhinolophus euryale*.
After Stanĕk, 1933.

3.3.2.3 Stapes

For all terrestrial mammalian species the stapes consists of a head, a neck, two crura (the posterior crus and the anterior crus) and a footplate. The crura of bats are deeply grooved, especially inferiorly where the crura join the footplate of the stapes. The central part of the footplate is more fibrous than bony.

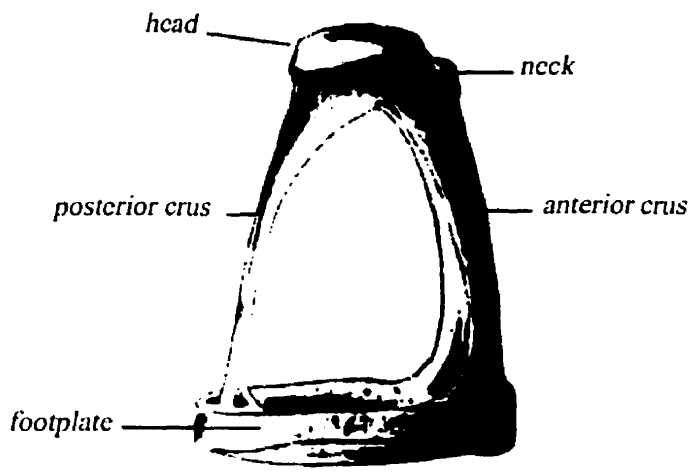

Figure 3.8
The stapes of *Rhinolophus ferrumequinum*.
After Staněk, 1933.

3.3.3 Muscles

The mammalian middle ear includes two muscles, the tensor tympani and the stapedius muscle, and both have striated muscle fibres. Recent observations have found that the annular ligament of the tympanic membrane of the moustached bat contains smooth muscle fibres (Henson & Henson, 2000). In this section an overview of striated and smooth muscle will be presented, as well as the anatomy and function of the two middle-ear muscles and the annular ligament.

3.3.3.1 Striated & smooth muscles

The organisation of striated muscles is highly structured. Individual muscle fibres are bundled by loose fitting endomysium. These bundles are packed together into larger units surrounded by a strong protective perimysium. The entire muscle consists of several bundles and is surrounded by a strong sheath, called the epimysium. Figure 3.9 presents a schematic overview.

Muscle fibres are made up of parallel myofibrils. The systematic arrangement of myofibrils gives the striated muscle its typical pattern, the so called cross-striations. The repeat unit of this pattern, called a sarcomere, contains actin and myosin filaments. Each individual fibre cell is cylindrical in shape, and about 10-100 microns in diameter (Guyton, 1991).

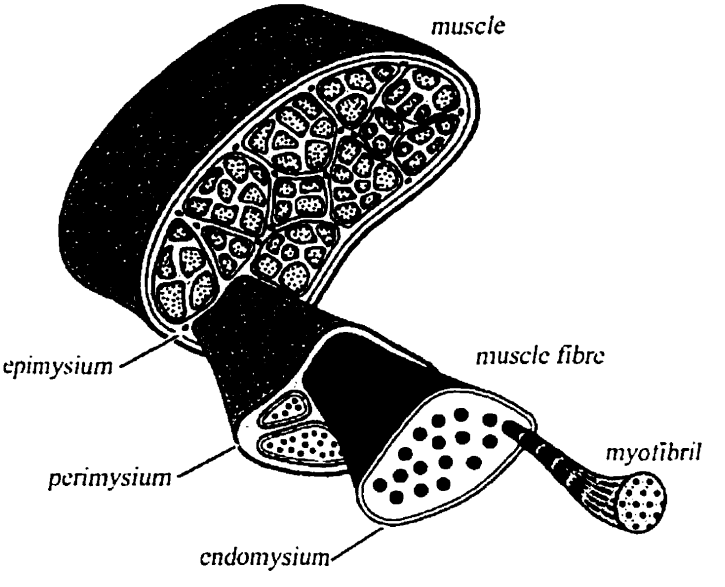

Figure 3.9
A schematic illustration of the different structures and substructures of a muscle.
After Nigg, 1999

Unlike most other cell types, striated muscle fibre cells contains hundreds of cell nuclei, each of which is situated just beneath the cell membrane.

In order to have an adequate supply of nutrients and oxygen, the muscle receives a rich blood supply which enters the muscle along the sides of the epimysium. To ensure an adequate blood supply through the entire muscle, tiny capillaries run between individual muscle fibre cells. To control the muscle's activity, the muscle is innervated by the muscle somatic nervous system.

The smooth muscle type is not striated. The characteristics of smooth muscle are highly dependent on the location, and thus function, of the particular muscle. They differ anatomically, functionally and mechanically but there are features common to all of them. All smooth muscles, like striated muscles, contain actin and myosin; rely on ATP for their energy supply; and use chemical changes in the cell membrane to induce ion fluxes and action potentials.

Smooth muscle cells are in general smaller than striated muscle cells, though the myosin filaments of smooth muscle are longer than those found in striated muscles. Fung (1993) concluded that the tension generated per filament in smooth muscle is about 40% larger than in striated muscle, based on the assumption that the cross-bridges of smooth muscle are similar to those of striated muscle. The higher tension per filament can be explained by the looking at the arrangement of the cross-bridges, which are in parallel, at equal spacing. Since the sum of the forces is proportional to the myosin fibre length, the tension will be larger.

Arterial smooth muscle generates a force which is comparable to that of skeletal muscle when normalised to the cross-sectional area, although smooth muscle has only about 20% of the myosin content when normalised by tissue weight (Murphy et al., 1974).

3.3.3.2 Tensor tympani & stapedius muscle

The tensor tympani is the largest muscle in the middle-ear. It is attached to the sphenoid bone, crosses the middle ear cavity, and is connected to the muscular process of the malleus. It receives its innervations from the motor root of the trigeminal nerve.

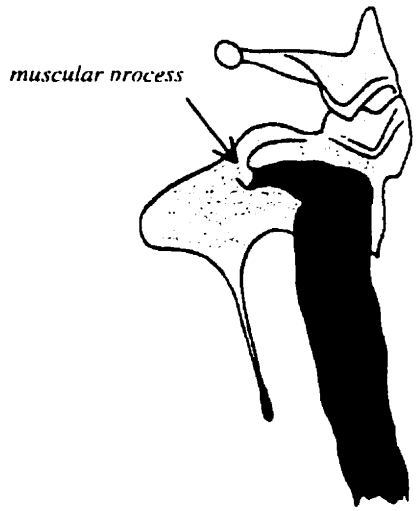

Figure 3.10
The tensor tympani connected to the malleus.
Nyctalus noctula After Staněk, 1933.

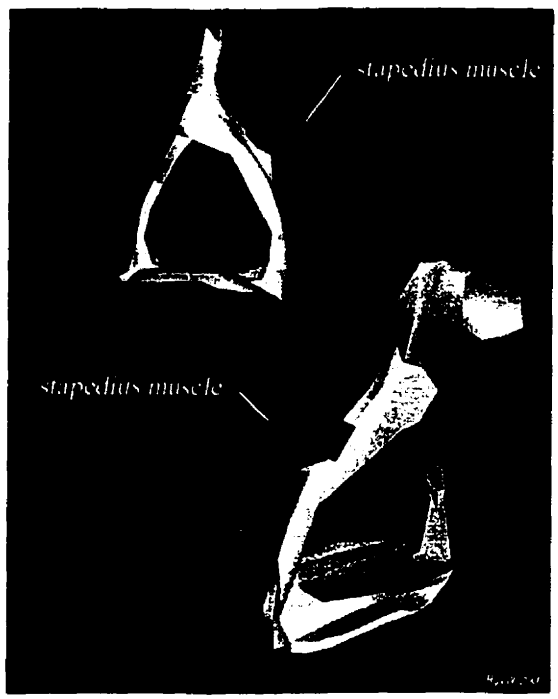

Figure 3.11
The stapedius muscle connected to the stapes.

The stapedius muscle is innervated by the facial nerve. The muscle starts at the walls of the stapedial fossa and is attached to the stapes by means of a single tendon which is connected to a muscular process on the posterior part of the head of the stapes.

3.3.3.3 Annular ligament

The annular ligament is a radially shaped ligament connecting the tympanic membrane to the tympanic ring. In mammals this ligament receives its blood supply through the numerous blood vessels which penetrate the ligament. It consists of radially arranged collagen fibres and numerous fibroblasts.

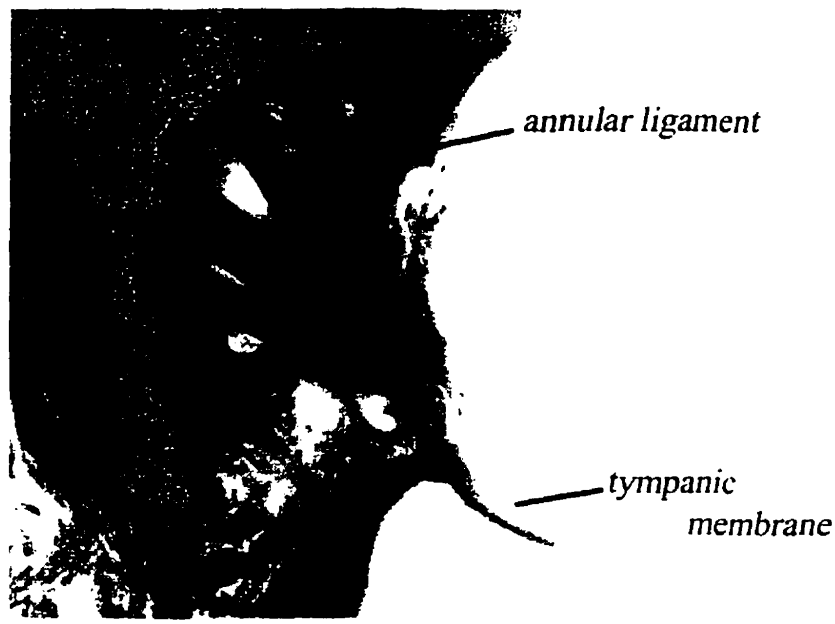

Figure 3.12 A close-up of the radial shaped annular ligament and tympanic membrane.

In addition to the fibres and fibroblasts, Henson & Henson (2000) recently reported the existence of a well-developed system of radially arranged smooth muscle cells. This system suggests the possibility of a tonic regulation of the tension of the tympanic membrane. The presence of smooth muscle fibres has also been confirmed for mice, gerbils, rats and hedgehogs (Henson et al., 2001a). In humans, the fibres are present, though not as common, and in a more complicated branching arrangement (Henson et al., 2001b).

3.3.3.4 Muscle function

The middle-ear muscles are particularly well developed in the bat. Wever & Vernon (1961) found that the mass of a cat's tensor tympani muscle is approximately half that of the ossicular mass. In some bat species the mass of the muscles is almost equal to that of the ossicular chain.

The function of the tensor tympani and stapedius muscles of bats has been studied by Henson & Henson (1972). They appear to start contracting 4 ms before pulse emission and to begin to relax during the terminal FM sweep of the pulse. The muscles completely relax 3 ms after the end of the pulse. The moustached bat has up to 20 ms of pulse-echo overlap, which means that the muscle contraction covers not only pulse emission but much of the echo reception as well. During the terminal phase of a goal-directed flight the repetition rate is so fast that the muscle will stay contracted and attenuation affects both pulse and echo. Thus there appears to be a continuous tension present in the muscle during emission and reception of the cry.

Chapter 4

FINITE-ELEMENT METHOD

4.1 Introduction

As previously mentioned, the mechanical behaviour of structures can be studied using the finite-element method. The elements into which the structure may be divided can have various shapes, such as rectangles, planes, beams, triangles, etc. Once the structure of interest is divided, the mechanical behaviour of each element is analysed. The elements are connected at specific nodes on their boundaries; the inter-element effects are taken into account at these nodes only. The response to the applied load is expressed in terms of the displacements of the element's nodes, which results in a matrix equation relating the behaviour of the element to the applied loads. The components of this matrix are functions of the shape and properties of that element. Finally all the element matrix equations are combined together into one overall system matrix equation.

The finite-element method has a number of attractive features. It deals with irregular boundary shapes very well, and it allows relatively easy handling of inhomogenities, non-linearities, and complex geometries and boundary conditions systematically. One never needs to analyse the whole system, because all the analysis is done on simple elements.

The programme SAP IV is used here for the finite-element analysis. SAP IV is a programme for structural static and dynamic response analysis of linear systems. The programme was developed by Bathe et al. (1973). It is written in Fortran and locally adjusted to suit the local requirements. It currently runs under Unix, Linux and Windows 95/98/NT.

The next section will discuss the Ritz-Rayleigh procedure including an example of a simple element analysis. Both are based on the description outlined by Stakgold (1968) and reiterated by Funnell (1975).

4.2 Ritz-Rayleigh procedure

The Ritz-Rayleigh procedure was introduced by Rayleigh in 1877 and generalised by Ritz in 1908. It is the most common procedure used for formulating finite-element approximations. The procedure is based on the theorem of minimum potential energy in mechanics. According to this theorem a functional giving the potential energy of a system has an admissible function which minimises that functional and is the solution of the system. An admissible function is one which satisfies the boundary conditions of the boundary-value problem, as well as certain continuity conditions.

A complete minimisation of the functional is difficult or impossible, so a limitation of the set of functions will be used to minimise the functional, leading to a set of admissible functions which can be expressed as:

$$w(x) = \sum_{i=1}^{n} c_i w_i(x) \tag{4.1}$$

were the c_i are n constants which define $w(x)$.

Let $F(w)$ be the functional over this set. Minimising $F(w)$ means that the c_i have to be chosen in such a manner that F is minimal. This can be done by taking the partial derivatives of F with respect to each c_i in turn and setting each to zero. The result is a set of n algebraic equations in c_i:

$$\frac{\partial}{\partial c_i} F(\sum_{i=1}^{n} c_i w_i) = 0 \qquad i=1, 2,.....n \tag{4.2}$$

Now the boundary-value problem is reduced to the solution of n linear equations in n unknowns.

4.3 Single-element analysis

As an example, a simple triangular plane-membrane element may be analysed by using three independent and admissible basis functions.

Equation 4.3 is a differential equation describing a plane membrane under tension and vibrating in a sinusoidal way:

$$T\nabla^2 w + \sigma \cdot \omega^2 w = p \tag{4.3}$$

where w is the membrane displacement in cm; σ is the area density; ω is the angular frequency; T is the tension; and p is the applied pressure.

The energy for this system may be expressed as

$$F(w) = \tfrac{1}{2}\iint |\nabla w|^2 \, dS + \tfrac{1}{2}\iint \lambda^2 w^2 dS - \iint w \cdot g dS \tag{4.5}$$

where the first integral represents the energy due to membrane tension, the second represents the inertia, and the third the applied pressure. The integrals are over the region of interest, here the single plane element.

This function may be minimised using the Ritz-Rayleigh procedure. Minimising may involve taking the set $\{1,x,y\}$ of basis functions which lets the displacement field over the element be a general linear function of x and y. The displacement at any point (x,y) can then be given by the linear combination of the functions:

$$w(x, y) = c_1 + c_2 \cdot x + c_3 \cdot y \tag{4.6}$$

The result of applying the Ritz-Rayleigh procedure to the expression is a set of algebraic equations for c_i:

$$\mathbf{A}\cdot\mathbf{c} = \mathbf{B}\cdot\mathbf{g} \tag{4.7}$$

in which **A** and **B** are functions of the vector coordinates of the triangular element (x_1, y_1, x_2, y_2, x_3, y_3) and of λ. The components of **g** represent the nodal values of the pressure field $g(x,y)$. This equation is valid for one element. To use this equation for a system with multiple elements the coefficients c_i must be transformed to nodal displacements using:

$$\begin{pmatrix} w_1 \\ w_2 \\ w_3 \end{pmatrix} = \begin{pmatrix} 1 & x_1 & y_1 \\ 1 & x_2 & y_2 \\ 1 & x_3 & y_3 \end{pmatrix} \cdot \begin{pmatrix} c_1 \\ c_2 \\ c_3 \end{pmatrix} \tag{4.8}$$

Expressing this in matrix notation gives:

$$\mathbf{w} = \mathbf{X}\cdot\mathbf{c} \tag{4.9}$$

where w_i are the nodal displacements. The equations express the nodal displacements as linear combinations of the basis functions. Combining this with equation 4.7 gives:

$$\mathbf{A}\cdot\mathbf{X}^{-1}\cdot\mathbf{w} = \mathbf{B}\cdot\mathbf{g} \tag{4.10}$$

where $\mathbf{B}\cdot\mathbf{g}$ is a vector of the nodal forces **f**, and the components of $\mathbf{A}\cdot\mathbf{X}^{-1}$ are the ratios of forces to the displacements, so that we may write:

$$\mathbf{S}\cdot\mathbf{w} = \mathbf{f} \tag{4.11}$$

where **S** is known as the element stiffness matrix.

4.4 Multiple-element analysis

If a system is to be analysed, multiple elements must be taken into consideration. Consider the system shown in figure 4.1, which consists of two triangular elements.

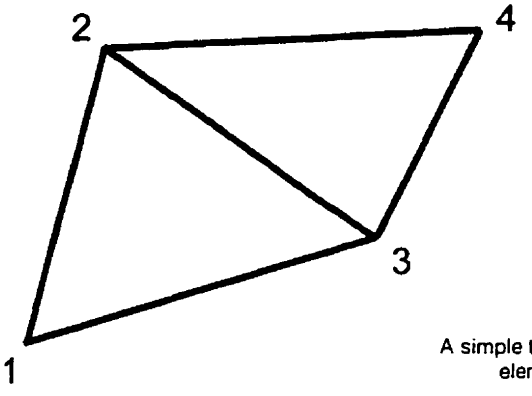

Figure 4.1
A simple two-element system with two triangular elements coupled at nodes 2 and 3.
After Funnell, 1975

For the first element, the components a_{ij} of the stiffness matrix **S** may be obtained by substituting the material properties and vertex coordinates into the equations obtained from the analysis. Formula 4.11 may now be written as

$$\begin{pmatrix} a_{11} & a_{12} & a_{13} \\ a_{21} & a_{22} & a_{23} \\ a_{31} & a_{32} & a_{33} \end{pmatrix} \cdot \begin{pmatrix} w_1 \\ w_2 \\ w_3 \end{pmatrix} = \begin{pmatrix} f_1 \\ f_2 \\ f_3 \end{pmatrix} \tag{4.12}$$

For the second element this leads to

$$\begin{pmatrix} b_{11} & b_{12} & b_{13} \\ b_{21} & b_{22} & b_{23} \\ b_{31} & b_{32} & b_{33} \end{pmatrix} \cdot \begin{pmatrix} w_2 \\ w_3 \\ w_4 \end{pmatrix} = \begin{pmatrix} g_2 \\ g_3 \\ g_4 \end{pmatrix} \tag{4.13}$$

The elements are connected at nodes two and three, so w_2 and w_3 in equation 4.12 are the same as w_2 and w_3 in equation 4.13. Therefore the two equations may be combined:

$$\begin{pmatrix} a_{11} & a_{12} & a_{13} & 0 \\ a_{21} & a_{22}+b_{11} & a_{23}+b_{12} & b_{13} \\ a_{31} & a_{32}+b_{21} & a_{33}+b_{22} & b_{23} \\ 0 & b_{31} & b_{32} & b_{33} \end{pmatrix} \cdot \begin{pmatrix} w_1 \\ w_2 \\ w_3 \\ w_4 \end{pmatrix} = \begin{pmatrix} f_1 \\ f_2+g_2 \\ f_3+g_3 \\ f_4 \end{pmatrix} \tag{4.14}$$

The actual displacements may now be calculated by solving the system matrix equation. This matrix equation represents a system of linear algebraic equations which can be solved in a number of ways. The most common ones are Gauss-Jordan elimination and Cholesky's method.

4.5 Dynamic models

The preceding analysis applies to static cases, but the more general dynamic case may be expressed as:

$$\boldsymbol{K} \cdot \boldsymbol{w} + \boldsymbol{C} \cdot \boldsymbol{w}' + \boldsymbol{M} \cdot \boldsymbol{w}'' = \boldsymbol{f} \tag{4.15}$$

in which $\boldsymbol{K}$ represents the static stiffness matrix, $\boldsymbol{M}$ the mass matrix, and $\boldsymbol{C}$ the damping matrix.

The simulations carried out for this thesis include static cases only.

Chapter 5

METHODS

5.1 Introduction

This chapter describes the different stages of modelling. First the Magnetic Resonance Microscopy (MRM) and histological data will be presented. Secondly, the process of segmenting the images and triangulating the model will be discussed.

5.2 MRM

5.2.1 Introduction

Magnetic Resonance Microscopy (MRM) is based on nuclear magnetic resonance (NMR). NMR is a modality for imaging proton densities and is currently used in both Magnetic Resonance Imaging (MRI) and MRM. Several publications discuss the principles of NMR, MRI and MRM (Curry et al., 1990; Zhou et al., 1995; Brown et al., 1999). MRI is a 3-dimensional diagnostic scanning method capable of displaying anatomy and pathological changes. It has set a new standard in diagnosis and has enhanced the level of care in modern medicine. The major advantage over other scanning techniques is that soft-tissue differentiation and boundary contrast between anatomical structures are both clearly visualised.

MRM is closely related to MRI and it can be seen as an extension of the MRI technique to microscopic dimensions. Due to advances in MRI technology the spatial resolution of images has increased, allowing for the microscopic study of structures. MRM offers some theoretical and technical challenges which are not encountered in MRI. For example, to reach the desired level of microscopic spatial resolution not only the digital resolution has to increase, but also other intrinsic resolution limits like linewidth broadening and diffusion have to be addressed. If digital resolution increases, the intrinsic resolution will determine the true image resolution. The intrinsic resolution is

often not a determining factor in conventional MRI. Technical challenges include the development of imaging pulse sequences specially focused on MRM. When resolution is increased, a much stronger gradient is needed. This too causes new technical challenges and leads to new phenomena not observed in conventional MRI.

5.2.2 MRM data

In order to create a model with a realistic 3-D geometrical shape the structures of interest have been segmented from two MRM data sets. The sets were made available by M. Henson & O.W. Henson, Jr., from the University of North Carolina at Chapel Hill. They were scanned at Duke University Center for In Vivo Microscopy.

The first set is one of a moustached bat (*Pteronotus parnelli parnellii*), subject number 12148, from Jamaica. The set consists of 199 transverse sections, each 184 by 177 pixels. The isotropic voxel set has a resolution of 32 μm/pixel arranged from inferior to superior.

The second set is from a moustached bat (*Pteronotus parnellii rubiginosa*), set number 16963, from Trinidad. The set consists of 256 transverse sections, each 256 by 256 pixels. The isotropic voxel set has a resolution of 25 μm/pixel arranged from superior to inferior. Figure 5.1 shows an example of a slice.

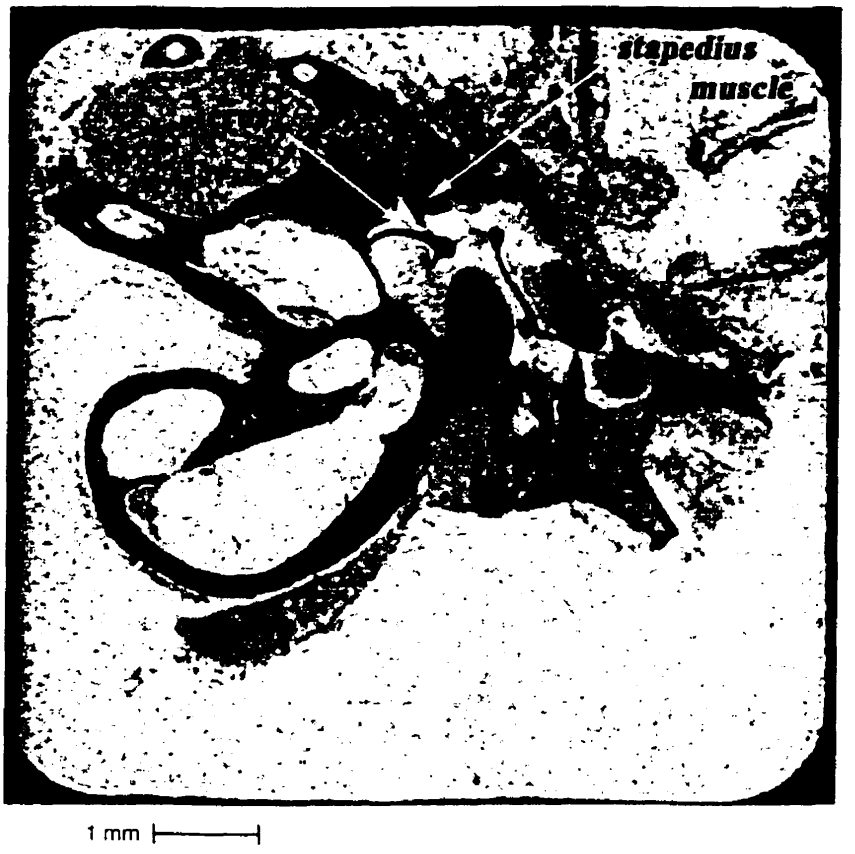

Figure 5.1 Slice number 110 from set 16963. The crus of the stapes and the connected stapedius muscle are highly visible.

The two MRM sets were used to create 3D-visualisation models and set 16963 was used to create the final finite-element model. Due to the resolution of 32 μm of set 12148 smooth tissues and tissue boundaries were hard to distinguish. Set 16963 was scanned at a resolution of 25 μm, however, which resulted in easier data analysis. For the latter, both muscles and tissue boundaries were highly visible, which was not the case for set 12148. Since the muscles are of major importance for the bat model, set 12148 has been used to create the final finite-element model.

5.3 Histology

5.3.1 Introduction

Histology is the science dealing with the microscopic identification of cells and tissue (Ham, 1969). The samples are prepared in such a way that different tissues can be distinguished from each other. Preparation of structures like the middle ear involves fixation, decalcification, embedding, sectioning, staining, and mounting.

First, the tissue has to be fixed in order to prevent the jelly-like proteins, which exist in large quantities in tissue, from washing away. The proteins are coagulated with formaldehyde. The next step is decalcification. The inorganic salts impregnated into the organic intercellular substance of bone and calcified cartilage are hard enough to cause difficulties in slicing the structure. To prepare the bone or calcified cartilage present within the block of tissue in such a way that it can be sliced, it needs to be decalcified. After the tissue has been fixed, it is therefore placed in a solution of decalcifying fluid, which dissolves the inorganic salts and leaves the organic intercellular substance behind. Now, the decalcified tissue has to be prepared permitting the tissue to be sliced without distortion. This can be done by replacing the decalcifying fluid present within the tissue with a sliceable material like paraffin. Finally, the slice is dried, stained, mounted with a medium which has a correct refractive index, and covered with a glass coverslip for protection.

The stains used here are hematoxylin and eosin. Hematoxylin is a natural stain which gives a blue to purple colour to the tissue with which it combines. Eosin is a synthetic stain, which appears pink to red, depending on the properties of the tissue.

5.3.2 Data

A set of histological serial sections was digitised in order to discern the fine details of soft tissues like the tympanic membrane, ligaments and muscles. The 152 sections are 20 μm thick and were digitised using a Kodak DC120 digital camera, with a resolution of 1280 x 960 pixels, and two light microscopes: a Carl Zeiss operating microscope with magnifications of 6 to 40, and a Zeiss Jena microscope with magnifications of 32 to 1000. The camera has been made compatible with the microscopes using adapters made by Kodak and Optem. From Kodak an MDS Universal adapter and an MDS 7mm spacer have been used. From Optem the adapter 1xSC10 25-70-17 has been used.

Figure 5.2 shows a histological slide of a part of the hearing system. The connective tissues are coloured pink to red, and the more solid structures, like bone and cartilage, are coloured blue to purple.

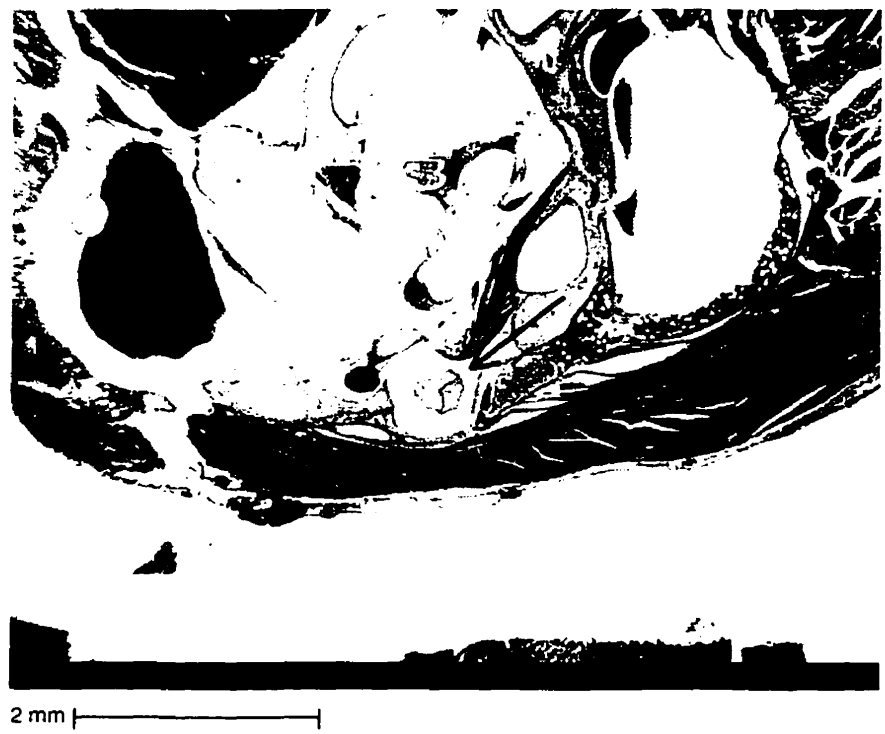

Figure 5.2: a digitized part of a histological slide of the moustached bat. The arrow points out the clearly visible boundary of the incudomallear joint.

The histology is a very useful complement to the MRM data, especially in defining the exact origins, insertions and dimensions of the ligaments. However, the histology is not used for the actual 3-D reconstruction because of alignment problems and, in some respects, the quality of the slides. Some structures are not present and some are folded. Figure 5.3 shows an example of a slide where part of the tissue is folded. This is due to the delicacy of the material and the complex procedure required to obtain the slides.

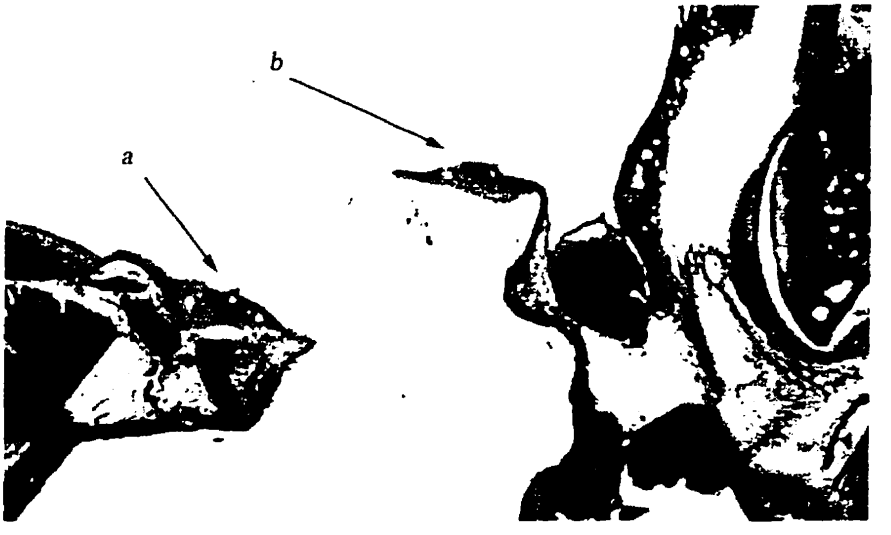

Figure 5.3: Enlargement of histology slide. Arrow *a* points to the undistorted part of the annular ligament. Arrow *b* points to the part of the annular ligament which is rotated by 180 degrees. The tympanic membrane in between is totally folded.

5.4 Segmentation

5.4.1 Introduction

Segmentation refers to the process of specifying regions of interest and extracting them from a data volume. In the process of data segmentation three stages can be distinguished: classification, parcellation, and surface extraction. Classification involves the assignment of a tissue-type label to pixels in an image or voxels in a data set. Parcellation is the clustering of the classified pixels and surface extraction is the excision of the structure.

Complex algorithms like region growing, active contours, and clustering algorithms, as well as more simple methods like thresholding and masking, are commonly used routines for segmenting the regions of interest.

The following sections will discuss some approaches to segmentation and will present the method currently used here for open and closed contour segmentation.

5.4.2 Edge-based segmentation techniques

Edge-based segmentation is a method which describes the resulting segmented image in terms of the boundaries between different regions. There are several edge-operators available: Laplacian-of-Gaussian (Marr and Hildreth, 1980), Sobel (Cornsweet, 1970), and Prewitt operators (Cornsweet, 1970). Often edge-detection techniques will result in a large number of small edge segments. To reduce this large number there has to be some kind of pre-processing done in the form of smoothing.

Active contours or "snakes" have recently grown in popularity. Snakes were introduced by Kass et al. (1987). Since then the algorithm has been developed further. Yu et al. (1995), for example, proved the validity of this method with experiments on medical volume images. The snake consists of a parametric curve which will be deformed under the influence of internal and external forces.

The internal forces depend upon the regularity of the contour. The external forces are related to image-dependent features like the local image gradient. The forces are fed into a cost function which is iteratively minimized and causes the snake to move to its optimal position.

The above-mentioned techniques were not employed in the creation of this model. This decision was made based upon the characteristics of the tissue and the image data. The structures of interest are very fine and delicate, which often causes the boundaries between different structures to be indistinct. The resolution of the image is not high enough to have a clear discrete view of the different structures. Segmentation algorithms are often based on two properties of grey-level values: discontinuity and similarity (Gonzalez & Woods, 1993). The presence of these two properties in the data set is not distinct enough to be used successfully.

5.4.3 Open and closed contours

For the process of segmenting the structures of interest, open contours are used here in addition to the usual closed contours. The technique is based on manual tracing of boundary edges.

A closed contour completely encloses the region corresponding to a structure, while an open contour can explicitly represent both the shared boundaries of structures and also very thin structures which are to be modelled as single layers. Figure 5.4 shows a schematic example of closed and open contours, and the advantage of shared surfaces. Figure 5.5 shows a segmented tympanic membrane consisting of one single layer.

In addition to sharing boundaries and modelling structures with single layers, surface definitions for complex or branching structures can be better controlled using open contours. These features are of great importance for finite-element modelling.

Figure 5.4

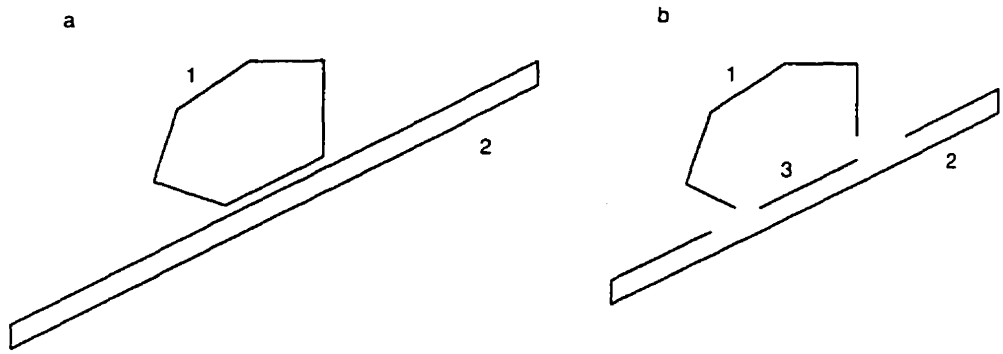

(a) shows two closed contours. Originally contour 1 should connect to contour 2, though due to the limitations of closed contours, they cannot have similar properties at the boundary.
(b) shows the same two structures, though this time traced with 3 open contours. At the boundary of the structures contour number 3 is part of structure 1 and part of structure 2. Structure one consists of contours 1 and 3 and structure 2 consists of contours 2 and 3.

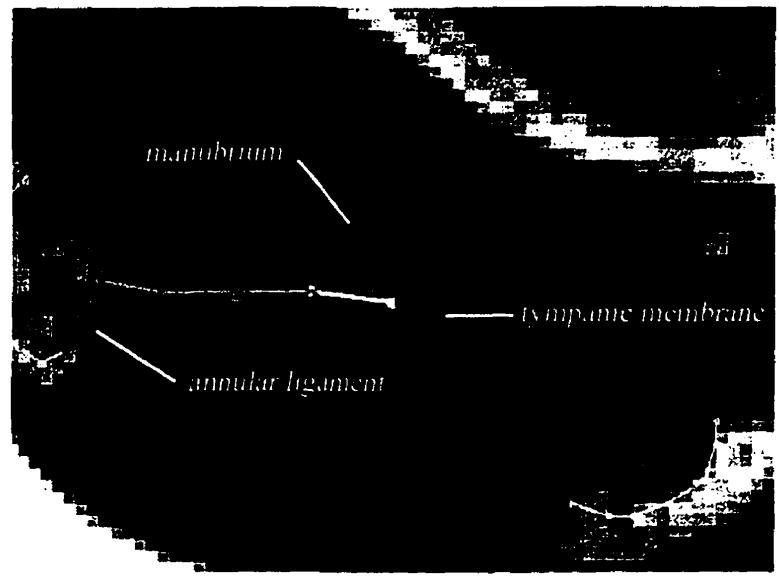

Figure 5.5: Part of an MRM image of subject 12148. Visible are the tympanic membrane, annular ligaments and manubrium. The tympanic membrane is segmented using three open contours providing the ability to have a shared surface with the manubrium.

One major disadvantage of manual tracing and the use of open contours is the labour-intensive nature of the process. At present each contour must be manually traced. Due to the architecture, multiple lines per structure are created. Keeping track of the definitions of all the structures requires a clear and distinct way of naming the structures.

5.4.4 Segmentation programmes

5.4.4.1 Introduction

Different programmes have been used to convert, segment and display the MRM data. The three most used are MNI-Display and Scion Image for displaying and orientation, and Fie for segmentation. What follows is an overview of the three programmes.

5.4.4.2 MNI-Display

MNI-Display was developed at the Montréal Neurological Institute (MNI) by David MacDonald (1995). The main purpose of the programme is to manipulate and display 3D-objects like cortical surfaces and sulcal curves. The programme runs under Unix and Windows 95/98/NT. Unfortunately, it can only handle the MINC file format, a file format defined by the MNI. The user interface makes use of combined keyboard and mouse controls. The program simultaneously displays three orthogonal views of the data, corresponding to the three slicing planes of the input volume. The program offers different manipulation tools: filters, colour coding tables, semi-automatic segmentation, and manual segmentation. The programme is limited to volume segmentations and cannot handle shared surfaces between structures. The programme has been used for displaying the different orthogonal views.

5.4.4.3 Scion image

Scion Image for Windows is the Windows version of NIH Image, a public domain image processing and analysis program for the Macintosh developed at the Research Services Branch (RSB) of the National Institute of Mental Health (NIMH), part of the National Institutes of Health (NIH).

Scion Image can acquire, display, edit, enhance, analyse and animate images. It reads and writes TIFF, PICT, and PICS files. It supports standard image-processing functions like contrast enhancement, density profiling, smoothing, sharpening, edge detection, and median filtering. The programme can be used to measure area, mean, centroid, perimeter, etc. of user-defined regions of interest. It performs automated particle analysis and

provides tools for measuring path lengths and angles. A tool palette supports editing of colour and grey scale images. It supports multiple windows and magnification. Segmentations can be stored in one of the three file formats. Unfortunately, these are not suitable for further processing with the programme for triangulation. Shared surfaces between structures cannot be defined. The programme has been used mainly for orientation purposes because it offers the possibility to skim quickly through image-stacks at any zoom level and to do oblique reslicing.

5.4.4.4 Fie

Fie is the programme which has been used here for segmentation. Fie stands for "Fabrication d'imagerie extraordinaire." It is a locally written programme which has been under development since 1989.

Fie is capable of various image-editing and related tasks (Herrera et al., 1991, 1997). It takes stacks of images in TIFF and raw format as input, and outputs a text file (.TR3) containing the different segmented structures in the form of nodal points of contours.

Within Fie two basic edge-detection algorithms are offered which are both based on examining the intensity profiles perpendicular to the user's initial tracing. One moves a template along the profile and attempts to maximise the correlation. The second algorithm determines where the profile either crosses a midrange value or has a minimum or maximum value. These algorithms turned out not to be useful. As mentioned before, the structures of interest are very delicate and fine causing frequent discontinuities of pixel intensities to appear. The two algorithms have difficulties dealing with the discontinuities. The programme can also use splines to modify and resample the shape of a contour based on given nodes.

The Fie programme runs under Unix, Linux, and Windows 95/98/NT. It is freely available and can be downloaded from http://funsan.biomed.mcgill.ca/~funnell/AudiLab/fie.html

5.4.5 Tr3 header

The text file generated by Fie contains information about the different connectivity parameters, material properties, and nodal points. The header contains the contour names which define the properties of the contours used. Four main parts can be distinguished: comments starting with semi-colons; contour definitions with their attributes; specific commands which control connectivity, material properties, etc. The header of the Tr3 file if dataset 16963 is included as appendix 1.

For the description of each contour the following standard has been developed. The description starts with an anatomical description of the contour, followed by the slice number on which the contour first appears. If the contour is part of a structure containing multiple contours all starting at the same slice a cardinal number will be assigned to the contour.

The following can be used to set the different parameters for each contour in the Tr3 file:

-o [***contour***]	[***contour***] may be OP for open contour or CL for closed contour
-c [***colour***]	[***colour***] may be a value between 1 and 7 1 white, 2 red, 3 green, 4 blue, 5 cyan, 6 magenta, 7 yellow, 0 black.
-r [***el/d***][***spacing***]	sets the parameters for the triangulation. [***el/d***] is the nominal number of elements per diameter and [***spacing***] is the parameter which sets the spacing between the slices which are read in for triangulation.
-t [***transparency***]	sets the transparency for the VRML output of the Tr3 programme. [***transparency***] may be a value between 0 and 1 with 1 being transparent and 0 being opaque.
-b [***boundary***]	sets the boundary condition. [***boundary***] may be C or F. C for clamped and F for free.
-m [***material***][***thick***]	[***material***] sets the material type as listed in MATERIALS, which is a section of the Tr3 file header. [***thick***] sets the thickness of the structure.
-p [***pressure***]	[***pressure***] is a multiplier which sets the pressure by multiplying a model-wide pressure value, currently set to 28.28 N/m^2 or dyn/m^2, depending on units of rest of model.
-s [***slocation***]	[***location***] establishes a connection between contours. **-s** is used to link the first node of the contour to a node of another contour. This can be the first, last or nearest node of the other contour using s, f, or n respectively.
-f [***flocation***]	[***location***] establishes a connection between contours. **-f** is used to link the last finish node of the contour to a node of another contour. This can be the first, last or nearest node of the other contour using s, f, or n respectively.

The next two examples are the definitions of contours 8 and 18.

Example one

8: -o OP -c 4 –t 0.5 -r 35 2 -m 4 5.u -b F –p 1.0 -s f 1 tm posterior 127

Contour 8 is a blue open contour. The transparency for VRML viewing is set to 0.5. The contour will be triangulated with 35 elements per diameter and every second slice is taken into account. The material type is set to 4 and the contour is 5 μm thick. The applied pressure is 1.0 * the acoustical pressure applied to the model. The starting point of the contour is connected to the end point of contour 1. The name of contour 8 is 'tm

posterior 127' and starts at slice number 127.

Example two

18: -o OP -c 7 -t 0.1 -r 150 1 -m 2 100.u -b F -p 0. -s s 27 -f f 27 malleus/incus 87 1

Contour 18 is a yellow open contour. The transparency for VRML viewing is set to 0.1. The contour will be triangulated with 150 elements per diameter and every slice is taken into account. The material type is set to 2 and the shell-element thickness is 100 μm. The boundary condition of the contour is free and the applied pressure is zero. The starting point of the contour is connected to the starting point of contour 27 and the end point of the contour is connected to the end point of contour 27. The name of contour 18 is 'malleus/incus 87 1', i.e. the contour is part of the 'malleus/incus', starts on slice 87, and is the first contour of a set of contours belonging to the structure.

The connections between contours are controlled by the so-called 'start at' (*-s*) and 'finish at' (*-f*) parameters, and the JOIN and MERGE commands. The first approach can connect the start and end points of a contour to the start and end points of another contour. This is established by setting the so-called 'start at' (*-s*) and 'finish at' (*-f*) parameters.

The MERGE command uses a technique which searches for the closest neighbouring node and merges the contours together. It merges structures present in the same slice, as well as in different slices, together. It can only handle two contours at a time. The syntax is as follows: first contour, second contour, and a parameter which sets the radius within which the programme searches for the presence of another contour. The following is an example of the MERGE command:

```
MERGE
99 28 2.          ; spring to stapes
```

This will merge contour 99 to contour 28 and will look for neighbouring nodes at a maximum distance of 2 pixels.

Contours may be connected between the different slices using the JOIN function. This function connects the two joining contours together by triangulating the boundary nodes of the two different contours. This function also offers the possibility of joining multiple contours at once. The syntax starts with a row number, a colon, the contour number(s) of the first structure, the word 'to', and the contour number(s) of the second structure. The direction of the contours of both the structures have to point in the same direction and are in order of appearance. Figure 5.6 shows an example. At the end of the line there is opportunity for a comment. The comment starts with a semicolon followed by the comment.

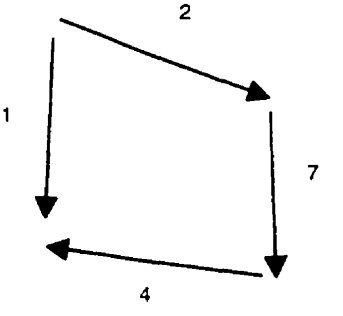

Figure 5.6: Schematic illustration of a structure. For the JOIN and CAP function the contours have to point in the same direction. The structure definition, starting at contour 2, will be as follows:

2 7 4 –1

Notice that contour number 1 has been reversed by the – sign.

Example

```
JOIN
3: 10 to 1 5 4          ; manubrium
```

Join number 3 joins two parts of the manubrium. The first part encountered in the stack consists of contour number 10, and the second part consists of contour numbers 1, 5 and 4.

Structures will begin and end with either 1-point contours or multiple-point contours. The surface reconstruction of a structure beginning or ending with a 1-point contour will not have an opening, but the reconstruction of a surface beginning or ending with a multiple-point contour will have an opening. The opening may be closed by using the CAP function, which caps the structure by triangulating its open area. The syntax consists of two parts: the parameter indicating which side of the structure to close, and the contour number or numbers representing the structure.

The first parameter is either HEAD or TAIL. Running through a stack of images from the beginning to the end of the stack, HEAD is used to cap that side of the structure which occurs first in the image stack, and TAIL is used to cap that side of the structure which occurs last. Similar to the JOIN function, the directions of the contours have to point in the same direction and are in order of appearance (Figure 5.6).

Example

```
CAP
TAIL 127 126 -125
HEAD 112 111 -110
```

In this example, the first structure to cap consists of contours 127, 126 and 125, and the cap must be placed at the end of the structure. Contour number 125 is in the opposite direction. To have all the contours looking in the same direction a minus sign has been added to contour 125.

The second structure consists of contours 112, 111 and 110, and the cap has to be placed at the beginning of the structure. Contour number 110 is in the opposite direction. To have all the contours facing in the same direction a minus sign has been added to contour 110.

The SPRINGS command represents elastic boundary conditions applied to the model. The SPRINGS command requires two contour numbers and a value for the spring stiffness preceded by the letter D.

Example

```
SPRINGS
103 104 D 1.
105 106 D 1.
```

The MATERIALS command supplies information about the material properties of the structures. The Young's modulus, the Poisson's ratio and density are set. The syntax is as follows. First the material number, then the Young's modulus, Poisson's ratio and density, and finally room for comments.

Example

```
MATERIALS
1 20.M 0.3 1000.   ;strong connective tissue (N/m2, kg/m3)
2 200.M 0.3 1900.  ;bone
3 2.M 0.3 1000.    ;soft connective tissue
4 20.M 0.3 1000.   ;strong connective tissue tympanic membrane
```

These are the four MATERIAL types used for the model of the middle ear of the bat.

5.4.6 Segmented MRM data

A rough segmentation of a portion of the structures in the form of a TIFF image stack came with the first data set, subject number 12148. This segmentation was carried out at the University of North Carolina at Chapel Hill with the programme NIH image.

a. b.

Figure 5.7: (a) MRM image 12148 slice number 114, (b) with the segmented areas.

To be able to read the segmented data with Fie and display the structure in VRML, a locally written conversion programme, written by Siah T.H. in our laboratory, has been used. This programme traces the boundaries and writes out a Tr3 file containing the coordinates of the pixels of the boundary. A data-reduction programme was then written in order to reduce the number of nodes. This programme runs through the list of nodes and eliminates redundant nodes, which are those nodes forming straight lines. Figure 5.8 shows an example of the difference between the original and reduced segmentations.

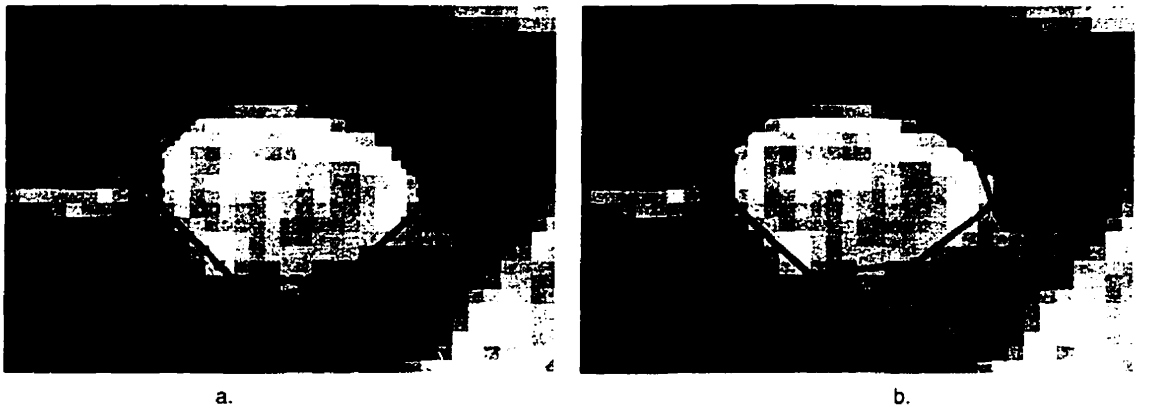

a. b.

Figure 5.8: Part of MRM image 12148 slice number 108 showing a segmented part of the malleus. (a) Shows the unreduced number of nodes, and (b) shows the reduced set.

The segmentation was found to be a very useful supplement in the identification and verification of the structures of interest. Despite this, the segmentation has not been used directly in the creation of the model. This decision was based primarily upon the fact that in many cases, two or more structures were combined into one structure. For example, Figure 5.9 shows that the annular ligament and tympanic membrane are combined. In addition, the tympanic membrane is segmented as hollow but should be modelled as a single layer.

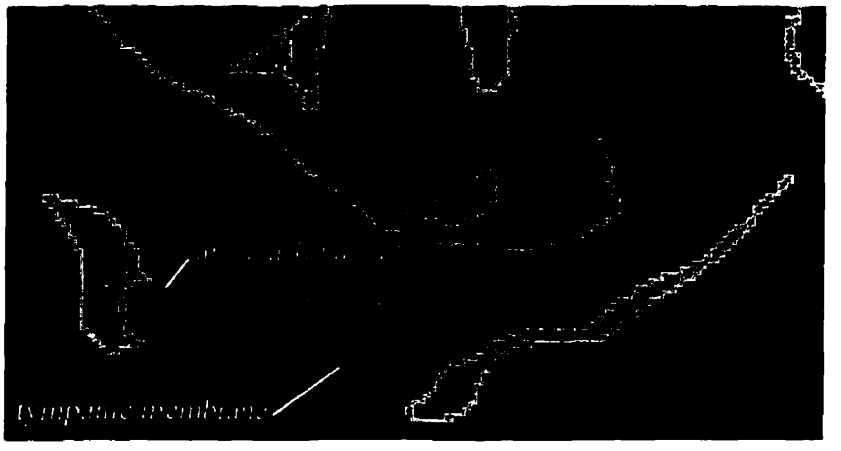

Figure 5.9: Part of the segmentation of slice 114 of subject number 12148.

5.5 Mesh generation

A mesh must be generated in order to analyse the structure using the finite-element approach. Mesh generation remains a challenge in finite-element modelling and many different approaches have been taken to create an optimum balance between computational demand and 3-dimensional geometry.

The Tr3 programme has been used to create the mesh. The programme has been under development since 1982. It is capable of triangulating 3-D surfaces between serial-section contours (Funnell, 1984a,b). Tr3 uses a (.tr3) plain-text model-definition file generated by Fie and optionally a tr3c control file as input and produces, among other output files, a VRML model file (.wrl) for 3D-visualisation purposes and a finite-element model file (.sap).

The Tr3 programme runs under Unix and Windows 95/98/NT. It is available for free and can be downloaded from http://funsan.biomed.mcgill.ca/~funnell/AudiLab/tr3.html

5.5.1 Mesh

The generated mesh consists of triangular thin-shell elements. Using thin-shell elements for thick structures, like the ossicles, is justified by the assumption that as long as the structure undergoes rigid-body motion only, no stresses and strains are induced within the structure. This approach does not represent a non-rigid bodies well. The only soft tissue used in the preliminary simulations is the annular ligament. The use of thin-shell elements for this structure is justified by the fact that the ligament is much thicker than the tympanic membrane and therefore effectively much stiffer than the tympanic membrane.

Each element is a triangle of arbitrary geometry and has six degrees of freedom: three translational and three rotational degrees of freedom.

The accuracy of the finite-element analysis depends on correctness, appropriateness of element formulations, and the resolution of the mesh. As the mesh resolution increases the displacement solutions will move towards the true displacements. On the other hand, as the size of the elements decreases the number of nodes increases and so does the number of degrees of freedom. This increases the size of the global stiffness matrix and load matrices and will affect the computation time. Figure 5.10 shows a graph of the computation time versus the number of nodes. Clearly visible is the non-linear increase of computation time with an increasing number of nodes.

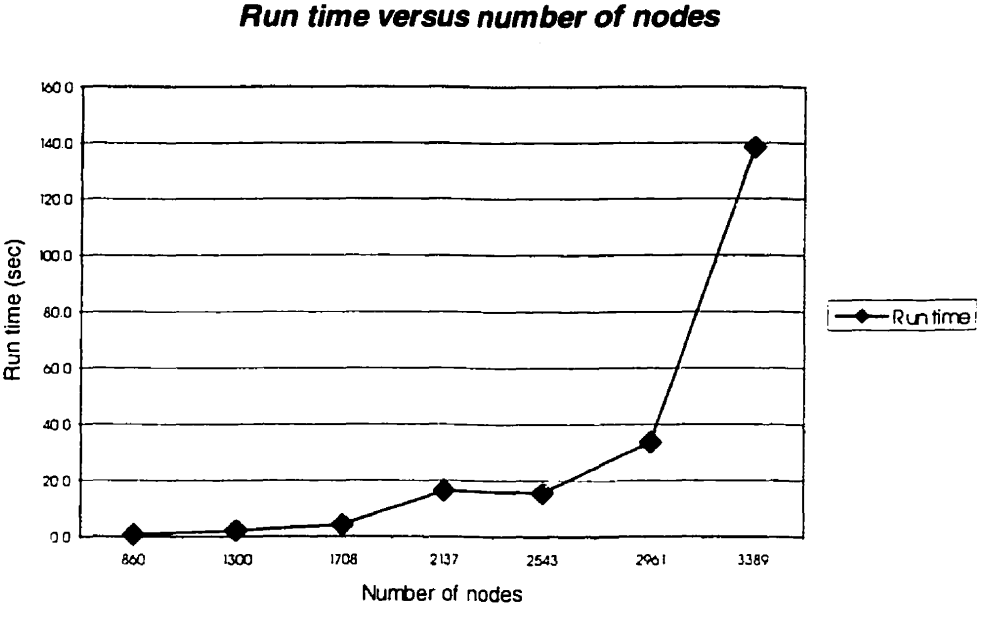

Figure 5.10: Graph of the total computational solution time versus the number of nodes. The data are from the simulations run for the convergence test described in Chapter 7.

5.5.2 *Bandwidth*

The computation time depends in part on the size of the bandwidth of the stiffness matrix. The bandwidth is the width of the band of non-zero numbers which lie about the diagonal of the stiffness matrix.

To minimise the bandwidth after the mesh generation, a bandwidth minimisation programme (Funnell, 1983) has been used. The programme renumbers the nodes in order to minimise the bandwidth, using the algorithm of Crane et al. (1976). It determines a rearrangement of rows and columns which leads to a rearranged matrix with a smaller bandwidth and profile. The size of the bandwidth has, in some cases, been reduced by as much as 95%.

5.5.3 *Node placement*

The action of the smooth-muscle fibres can be modelled by applying a radial load to the boundary of the model of the tympanic membrane. Each boundary node will have a load vector tangential to the tympanic membrane.

Figure 5.11 (a) shows an MRM image of the middle ear with the tympanic membrane and the annular ligament. The direction of the load vector is indicated by an arrow on the left side. Figure 5.11 (b) shows an enlargement of a digitised histological slide with the annular ligament clearly visible. The direction of the load vector is again indicated by an arrow.

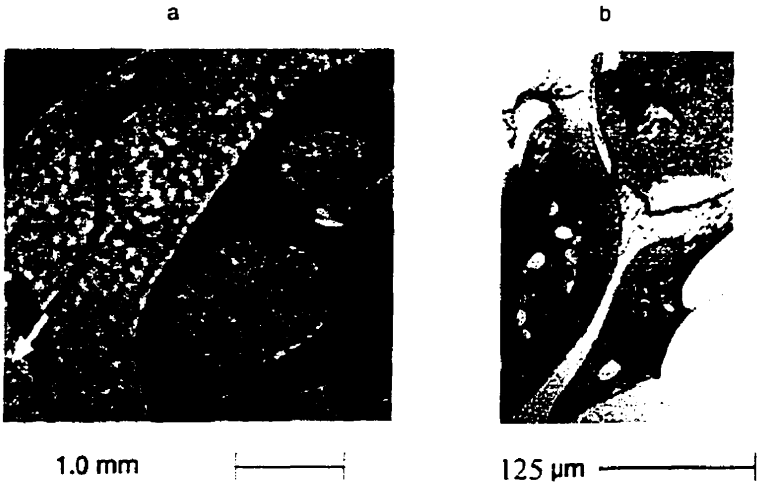

Figure 5.11: (a) MRM image of the middle ear with the tympanic membrane and the annular ligament, and the direction of the load vector indicated by an arrow on the left side. (b) An enlargement of a digitized histology slide with the annular ligament and the direction of the load vector again indicated by an arrow.

A feature has been added to Fad, a home-grown programme for manipulating 3-D finite-element models. The original programme has been under development since 1977. With the new feature added, it is now capable of calculating the positions and directions of the concentrated loads around a structure.

The concentrated loads are determined by the programme, which receives the specified material type as input and calculates the load vectors to which the concentrated loads must be applied. It identifies all the boundary edges of the structure with the enabled material type by discarding the edges which occur twice. Once the boundary edges are detected the positions of the boundary nodes can be acquired and the direction of the load vector can be determined. The load vector is calculated by taking the sum of the adjacent nodes and normalising the obtained vector. The information is written to the input file for SAP IV.

Chapter 6

THE FINITE-ELEMENT MODEL

6.1 Introduction

The finite-element model which has been created is a simplification of both the anatomy and the behaviour of the middle ear. This simplified model is sufficient for the first preliminary simulations, and may also be used to represent experimental data which might become available in the future. The model consists of the tympanic membrane, annular ligament, malleus and incus, stapes, tensor tympani and stapedius muscles, part of the temporal bone, springs which represent the load of the inner ear, and load vectors representing the applied load due to the muscle fibre surrounding the tympanic

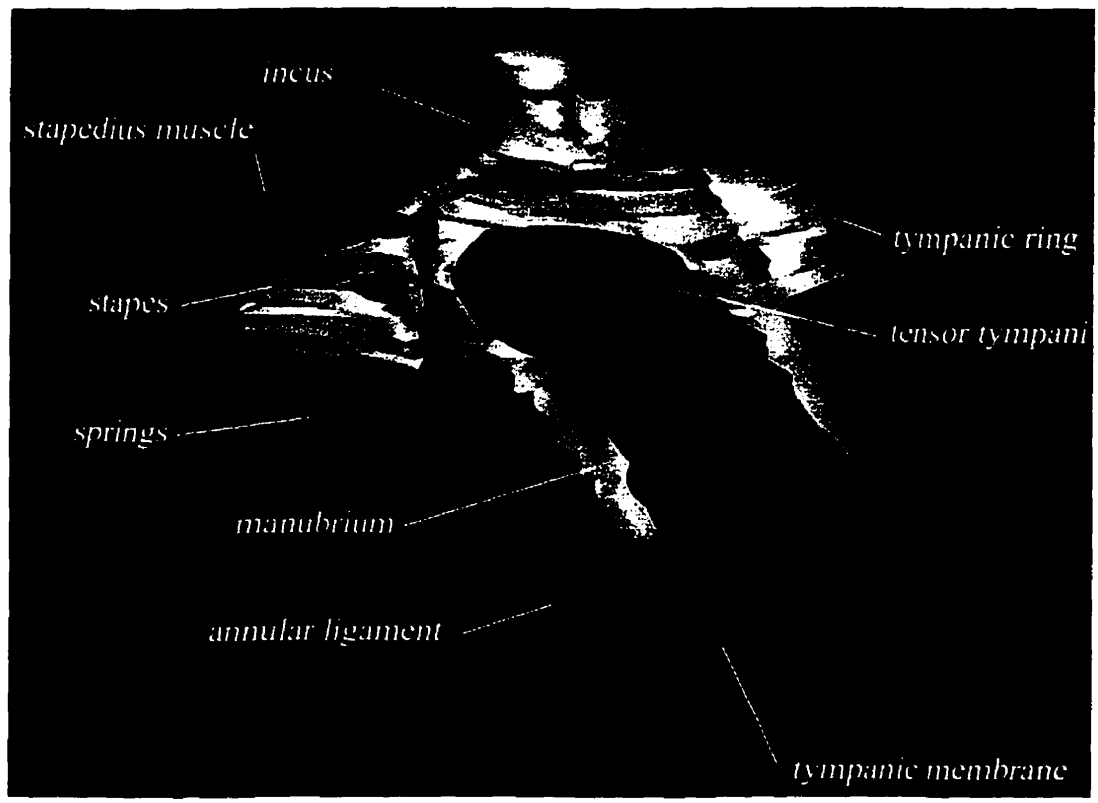

Figure 6.1: A VRML representation of the complete model. Visible are the annular ligament, tympanic ring, ossicular chain, eardrum, stapedius muscle and tensor tympani muscle, and springs representing the annular ligament of the stapes and the cochlear load.

membrane.

The structures are defined using the following mechanical properties: Young's modulus, thickness, material density, and Poisson's ratio.

The Young's modulus is a material stiffness parameter. When a longitudinal force is applied to a solid bar its length changes. The relative length change or longitudinal strain,

$$\varepsilon = \frac{\delta}{L_0} \tag{6.1}$$

is proportional to the applied stress σ:

$$\sigma = Y \cdot \varepsilon \tag{6.2}$$

where Y is the Young's modulus in N/m^2. This parameter varies for different materials. Some examples are: diamond 1000 GN/m^2, iron 196 GN/m^2, copper 124 GN/m^2, aluminium 69 GN/m^2, polyesters ranging from 1 to 5 GN/m^2, and rubbers ranging from 0.01 to 0.1 GN/m^2.

The Poisson's ratio is a dimensionless ratio. When a longitudinal force is applied to an isotropic solid bar, it also tends to change its dimensions in a lateral direction. The Poisson's ratio υ is a measure of the lateral strain against the axial strain when a uniaxial stress is applied. The Poisson's ratio is the relative length change along the two perpendicular directions:

$$\upsilon = -\frac{\Delta w}{w} \cdot \frac{\delta}{L_0} \tag{6.3}$$

Values for υ are 0.1 for rocks and 0.5 for rubbery materials. A sensitivity test conducted by Funnell (1975) showed that varying the Poisson's ratio in the model had little effect on the behaviour of the model.

6.2 Tympanic membrane

The tympanic membrane has been modelled as a uniform, homogeneous curved shell. This results in disregarding the possible mechanical implications of the highly organized layered structure (Funnell & Laszlo, 1982). The model also ignores any heterogeneities of the tympanic membrane and supporting structures. Since the surface area of the pars flaccida is relatively small in comparison to that of the pars tensa there is no distinction made between the two.

There is no available experimental data for the bat pertaining to the mechanical properties of the tympanic membrane. Preliminarily, some of the mechanical properties have been chosen to be the same as in our previous models (Funnell, 1996) which results in a Young's modulus of 20 GN/m^2 and a Poisson's ratio of 0.3. The thickness of the tympanic membrane in bats ranges from 110 μm to 20 μm (Henson 1970). Based on this and the histological data, the thickness is estimated at 25 μm.

The tympanic membrane has been segmented by defining the membrane with a maximum number of six nodes per slice and then applying a spline algorithm to obtain an approximation of the shape. This approach has the advantage that distortions due to the preparation of the specimen for the MRM scan are avoided. It results in a smooth and reasonable estimate of the structure. Figure 6.2 shows examples of the distortion.

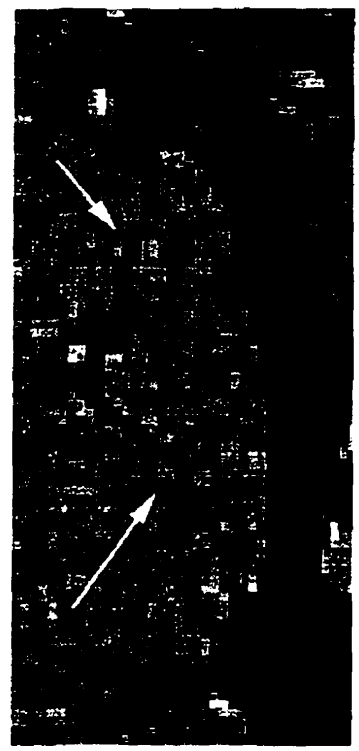

Figure 6.2

Section of slice 156 of subject 16963. The arrows point to distortions caused by the preparation of the specimen.

Figure 6.3a presents a side view of a triangulation and Figure 6.3b shows a side view which has been cut to emphasise the depth of the cone. Both are generated by Tr3 and visualised by Fad. The depth of the cone is greater than in many other species (Henson, 1970), including the human, cat and gerbil.

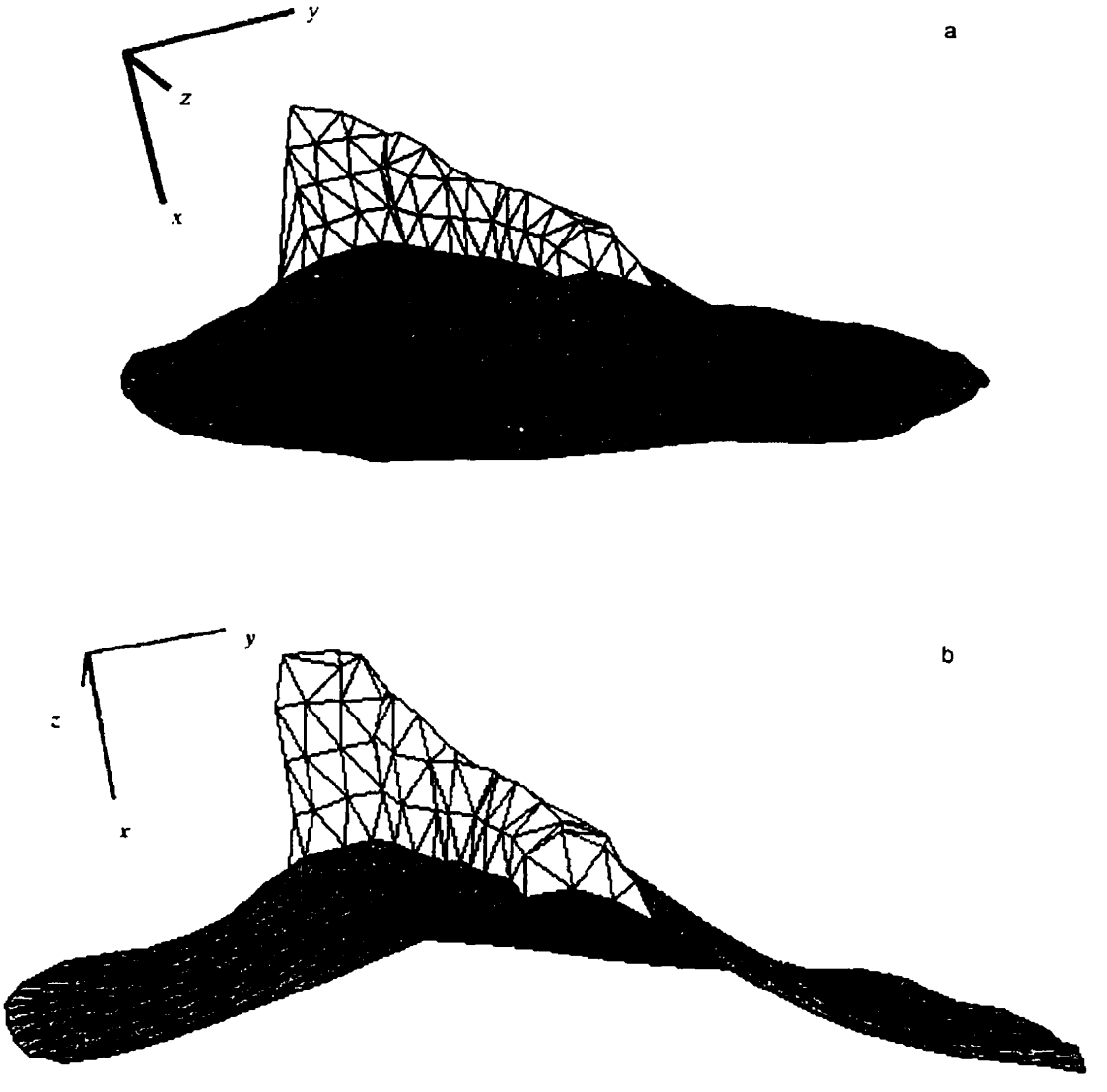

Figure 6.3 Side views of (green) the tympanic membrane and (yellow) the manubrium. The triangulation was carried out with 35 elements per diameter and a slice spacing of 2.

6.3 Annular ligament

As a preliminary estimate of the force generated by the smooth muscle tissue present in the annular ligament, a comparison has been made with the maximal force generated by the cat's stapedius muscle, which is approximately 3 g (Wever & Lawrence, 1954).

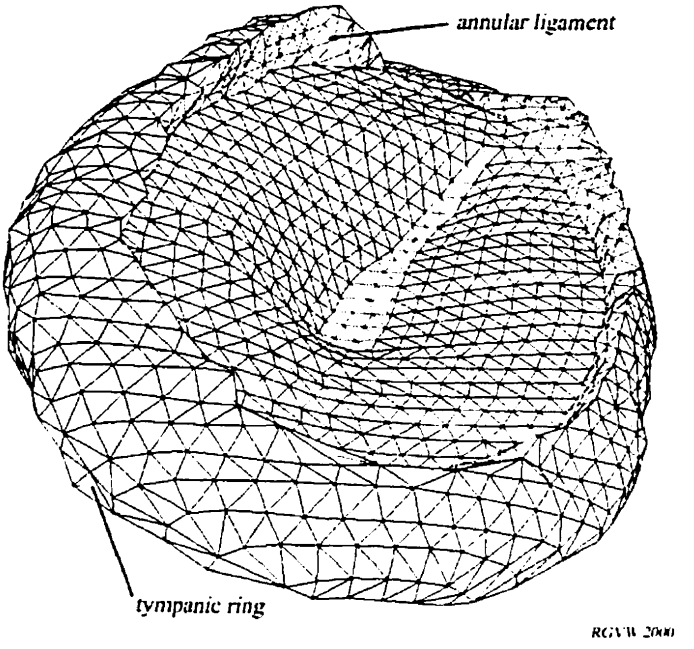

Figure 6.4: Triangulation of the tympanic ring, annular ligament, tympanic membrane, and manubrium.

The force generated by smooth muscle is comparable to that of skeletal muscle when normalised to the cross-sectional area (Murphy, 1974). A comparison of the cross-sectional area of the stapedius muscle with that of the annular ligament was made and resulted in a total applied radial load of 2.3 mN. This assumption was made because there are no available experimental data for the bat at this point.

6.4 Ossicular chain

Contractions of the middle-ear muscles occur around 85 dB SPL. During echolocation the bat emits sounds with intensities higher than 85 dB SPL. The interval between emission and reception of the cry is too short for the muscles to relax, which results in a continuous tension of the muscles. For now, however, no muscle activity is assumed to be present.

The assumed material stiffness of the ossicles is 200 GN/m^2 (Funnell et al., 1992). This estimate was based on several studies of bone stiffness and assumes a uniform bone density. This is in fact not completely true because the ossicles have less dense bone in the interior, which may reduce the overall stiffness.

Bone is a solid structure and should be modelled as a volume with solid elements. Due to the limitations of the mesh-generation programme which, at this point, is unable to mesh solid structures, this initial representation contains only shell elements forming a hollow shell. An advantage of this approach is that a hollow shell representation contains fewer nodes.

Figure 6.5: Medial view of the combined malleus and incus, and tympanic membrane.

6.4.1 Malleus & incus

The malleus and incus are modelled as a single rigid structure (Figure 6.5). The justification of this representation is based on Von Békésy's (1960) observation that for low frequencies the ossicles appear to be acting as a single rigid unit. Although not considered in this model, the motion of the ossicular chain and tympanic membrane becomes more complex for higher frequencies and is somewhat more complex even for low frequencies (Decraemer et al., 1989, 1991, 2000).

6.4.2 Stapes

The annular ligament of the stapes and the cochlear load are modelled as four springs (Funnell, 1996).

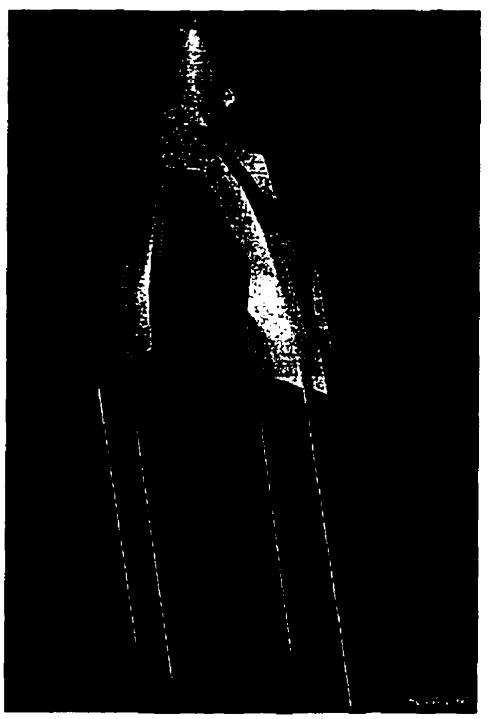

Figure 6.6: Medial view of the stapes with four springs attached to the footplate acting as loads.

6.5 Material behaviour

The model assumes linearly elastic material behaviour, despite the fact that most biological structures are viscoelastic (e.g., Özkzya & Nordin, 1991). In biological structures made up of fibres composed of collagen, elastin and other proteins, the architecture of the tissue evokes mechanical responses which are loading-path and rate dependent and are therefore non-linear and viscoelastic.

At all frequencies vibrations appear to be basically linear up to intensities of 130 dB SPL or more so long as contractions of the middle-ear muscles are not present (Guinan & Peake, 1967).

6.6 Acoustical input

As acoustical input a homogeneous sound pressure level of 120 dB SPL is applied to the tympanic membrane. The sound pressure level of 120 dB SPL is equivalent to a sound pressure of 28.28 N/m^2. The frequency is taken to be low enough that the inertial and damping effects may be neglected.

There is no acoustical load due to the middle-ear cavities, which are considered to be completely open.

6.7 Overall mesh

Figure 6.7 shows a medial view of the 3D-triangulation of the model generated by the Tr3 programme. The nominal number of elements per diameter is 35 and the slice spacing is set to 2. The tympanic ring lies in the y-z plane.

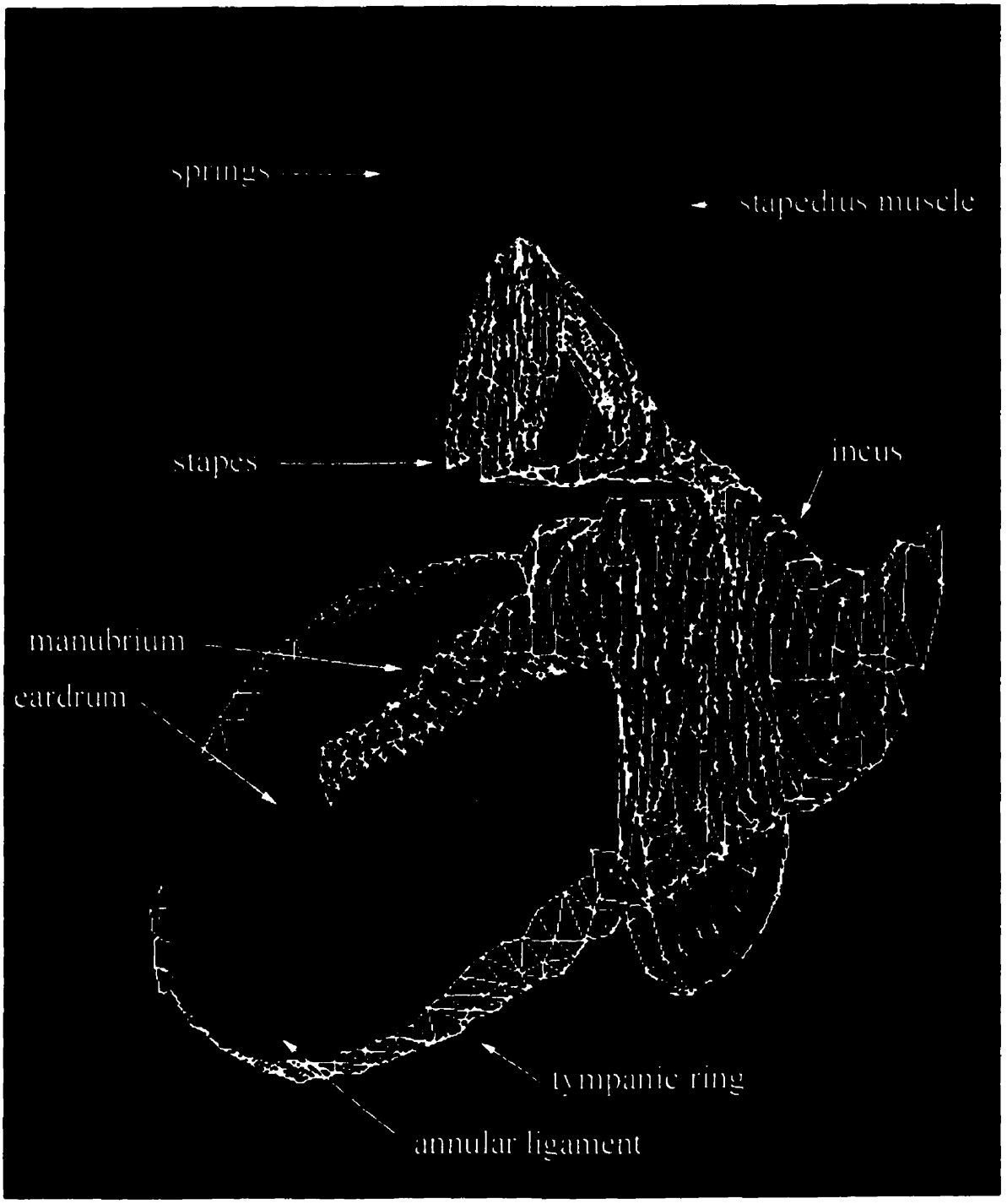

Figure 6.7: Triangulation of the model.

Chapter 7

RESULTS

7.1 Introduction

The following section presents the results of simulations carried out with the model of subject number 16963. Section 7.2 presents the simulations carried out to investigate convergence. In Section 7.3 the static displacements are measured. Section 7.4 reveals the sensitivity to tympanic-membrane shape and the effects of pressure and radial loads are presented in section 7.5.

All the preliminary simulations were carried out with the manubrium clamped, although it is recognised that clamping the manubrium is an over-simplification. Section 7.6 presents a simulation with an unclamped manubrium. Clamping the manubrium has the advantage of allowing us to focus purely on the displacement patterns of the tympanic membrane. By clamping the manubrium these displacements are relatively unaffected by variations in the ossicular load (Funnell, 1996b) and the corresponding manubrial motions.

Simulations show that clamping the annular ligament has little influence on the displacement pattern, with an overall displacement amplitude difference of less than 1%. Simulations of the tension of the annular ligament in section 7.5 have been carried out with an unclamped annular ligament; the remaining simulations have the annular ligament clamped.

7.2 Convergence test

The behaviour of the model changes as a result of varying the mesh resolution. A finer mesh resolution results in a more detailed model. The choice will always remain a compromise between accuracy and computational expense.

A suitable mesh resolution has been determined by generating the model with different mesh resolutions and running a convergence test sequence where the maximum and minimum displacements are plotted as a function of the number of elements per diameter.

The lower limit is set to a nominal number of 15 elements per diameter. Due to the limitations of Fie the connectivity between the different contours of a shell representation are lost if a smaller number of elements per diameter is used.

The results of the test set are shown in Figure 7.1. The curves for all except the maximum y component reach a plateau level between 30 and 45 elements per diameter. After 45 elements per diameter the magnitudes of all the components except the maximum z component decrease in value.

A finer mesh resolution should result in a more accurate model, which should result in a model which converges if the number of elements per diameter increases. Figure 7.1 shows that the model does not converge. Possible causes may be the lack of smoothness of the model or numerical instability due to the changing shape of the elements. The latter is less likely than the former because the curve is quite smooth, while sharp peaks and valleys could be expected if the problem lay with numerical instability.

To investigate whether the lack of smoothness of the model is the problem, an additional convergence test was carried out. The model was rotated in such a way that the tympanic ring was approximately parallel to the x-y plane, the z coordinates were multiplied by zero, and the boundary nodes of the tympanic membrane were clamped. The results of these simulations are shown in Figure 7.2 and show that the flattened model converges. The large displacement at 100 elements per diameter occurs at the boundary between two joined structures, and this might be due to an error during triangulation.

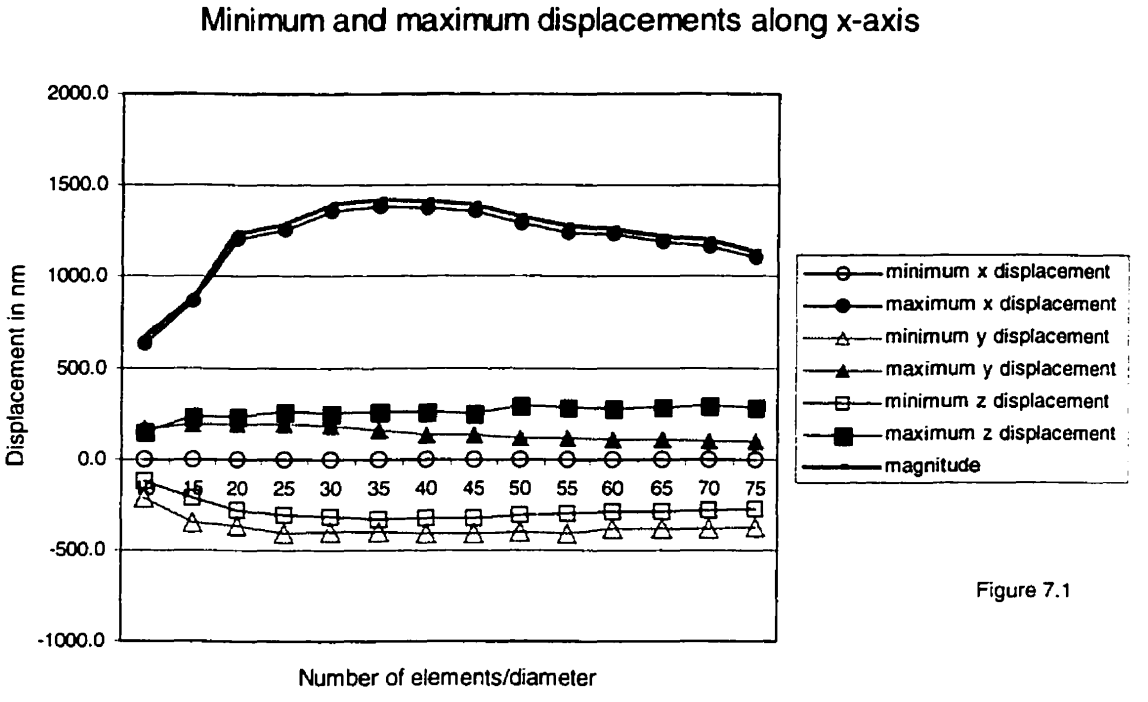

Figure 7.1

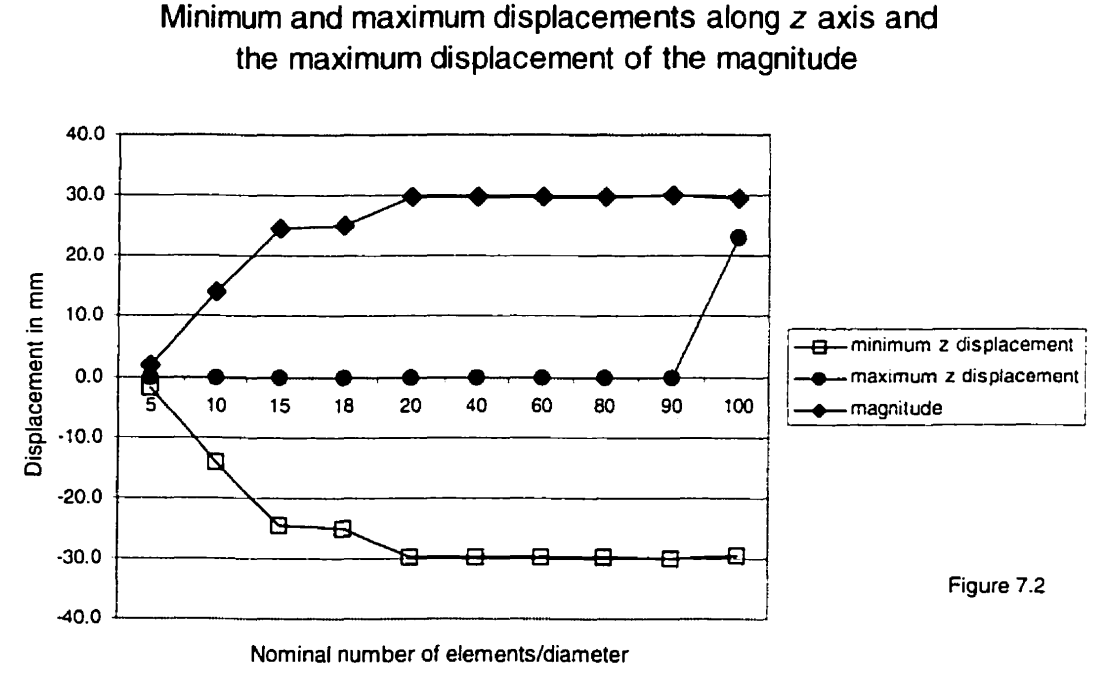

Figure 7.2

Based on the results, we have chosen to use a mesh resolution of 35 elements per diameter. The chosen mesh resolution is approximately the same as the mesh resolution of the model of the cat (Funnell, 1996). The displacements do not converge for different mesh resolutions. This behaviour is unexpected and, according to the results shown in Figure 7.2, might be due to the irregular shape of the surface of the tympanic membrane.

7.3 Static displacements

Figure 7.4 shows the low-frequency displacement patterns of the model. The displacements are normalized and colour coded, with zero being black, the maximum displacements being white, and negative displacements being red. The multiple peaks of displacement occur partway between the manubrium and the annular ligament. The x component is much greater than the y and z components. This is because of the orientation of the model. The plane of the tympanic ring is approximately perpendicular to the x axis, so the net force due to the pressure is approximately parallel to the x axis.

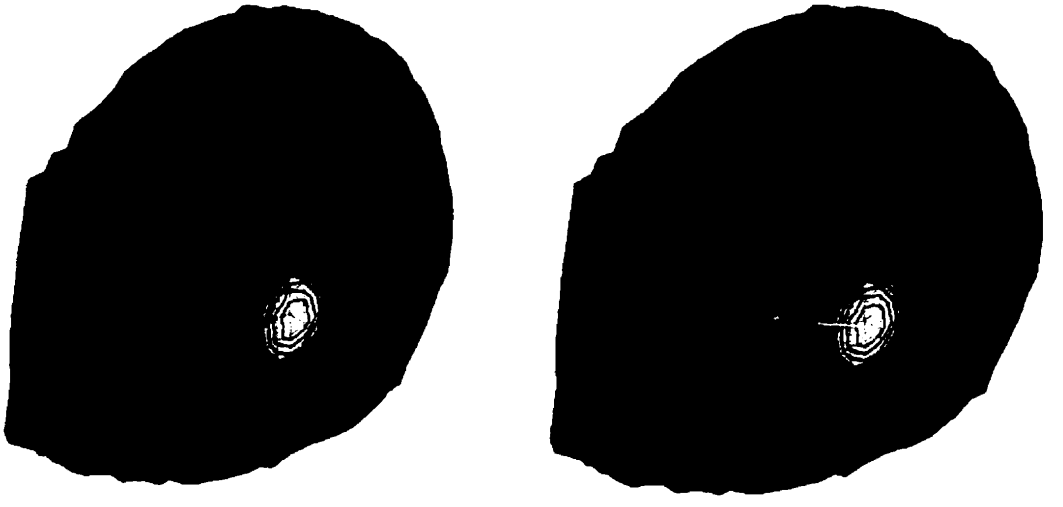

a

Minimum x displacement: -5 nm
Maximum x displacement: 1387 nm

b

Maximal displacement magnitude: 1427 nm

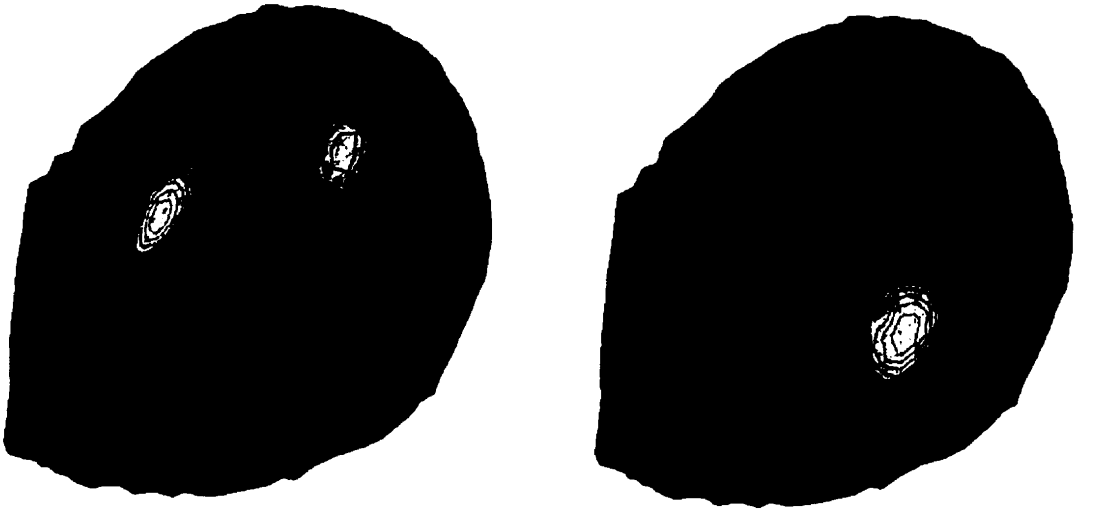

c

Minimum y displacement: -398 nm
Maximum y displacement: 157 nm

d

Minimum z displacement: -330 nm
Maximum z displacement: 255 nm

Figure 7.3: Visualisation of the displacement patterns along the different axes, and of the displacement magnitude, with the manubrium and the annular ligament clamped. The slice spacing is set to 2 and the nominal number of elements per diameter is 35.

7.4 Effects of tympanic-membrane shape

The effects of the distortion of the tympanic membrane caused by the preparation of the specimen have been investigated (see section 6.2). A static simulation with a manually segmented tympanic membrane has been compared with a simulation of a segmentation using the spline-interpolation technique. Figure 7.4 shows the two simulations. The displacement is about 70% less for the manual segmentation and the pattern is clearly different.

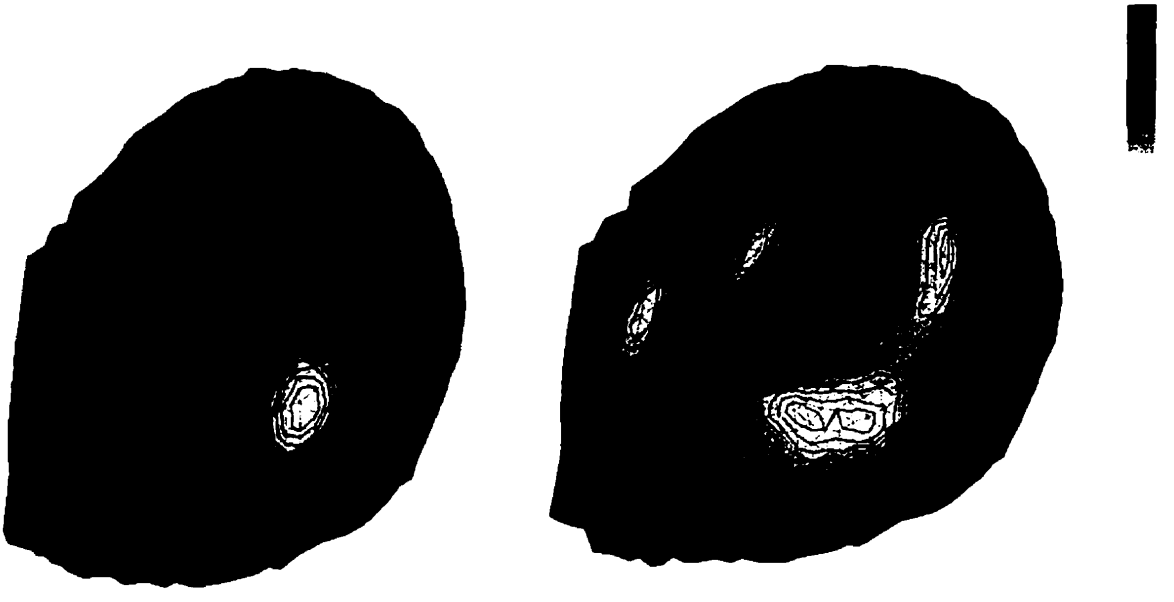

a b

Figure 7.4: Visualisation of the displacement patterns along the x axis with the manubrium and the annular ligament clamped. The slice spacing is set to 2 and the nominal number of elements per diameter is 35. (a) Spline-interpolated tympanic membrane (same as in Figure 7.3a). (b) Manually segmented tympanic membrane.

7.5 Effects of smooth muscle in annular ligament

A preliminary simulation has been carried out to explore the effect of the smooth muscle present in the annular ligament. The displacements parallel to the *x* axis for a radial load, alone, and for a combination of the applied sound pressure and the radial load are shown in Figure 7.5a and 7.5b. Figure 7.5c shows a simulation with only the applied pressure. Combining the pressure and the radial load causes the overall magnitude of the displacements to be about 4.6% greater than those for the sound pressure alone. The displacement patterns remain similar to those with only the applied sound pressure: Figure 7.5b versus 7.5c.

The total pressure applied is 28.28 N/m^2 and the total radial load applied is 2.3 mN. The surface area of the TM has been estimated at $2x10^{-6}$ m^2 which leads to a resulting applied force due to the sound pressure of 57 μN which is much smaller than the force of the applied radial load. The magnitude of the maximum displacement for the radial load is nonetheless only about 60 % of that for the sound pressure.

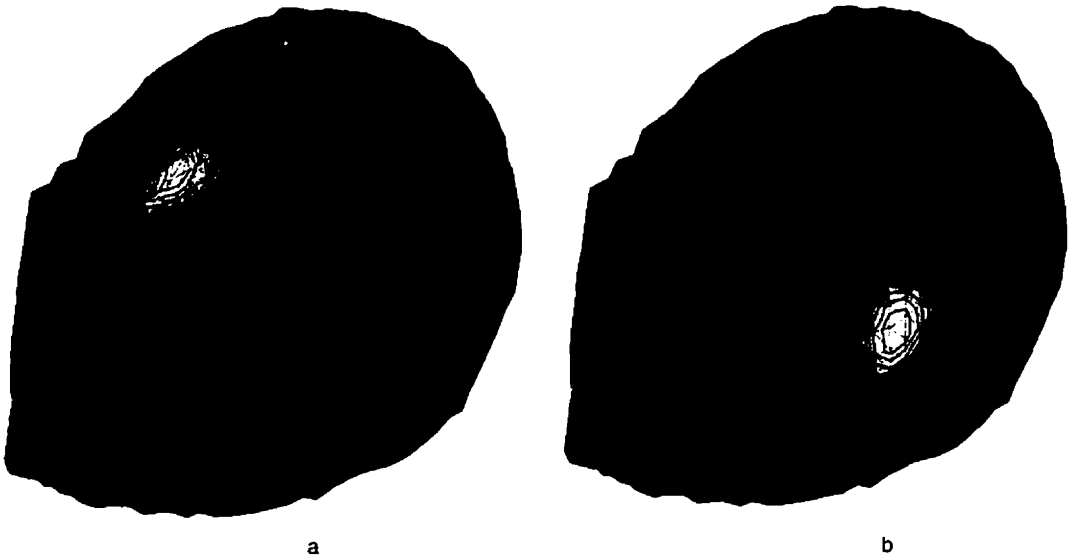

a b

c

Figure 7.5: Three visualisations of the displacements along the x axis for (a) an applied radial load; (b) an applied radial load and applied pressure; and (c) only an applied pressure (same as Figure 7.3a). For all the three simulations the manubrium is clamped. The slice spacing is 2 and the nominal number of elements per diameter is 35.

Simulation	Minimum *x* displacement	Maximum *x* displacement
(a) Radial load	-411 nm	268 nm
(b) Radial load + Pressure	-183 nm	1424 nm
(c) Pressure	-5 nm	1387 nm

7.6 Unclamped manubrium

The preliminary simulations have all been carried out with a clamped manubrium. The effect of an unclamped manubrium is simulated here. Figure 7.6 illustrates the displacement of the eardrum with the manubrium unclamped and not connected to the rest of the ossicular chain. Compared with simulation with the manubrium clamped, the largest displacements are still partway between the manubrium and the annular ligament and the maximum displacements occur in similar places. The displacements on the manubrium are smaller than on the neighbouring tympanic membrane. The maximal x displacement is about 70% greater than with the manubrium clamped. The locations of the maximum and minimum displacements are comparable with the patterns seen in those of the gerbil, cat and human.

Figure 7.6: A visualisation of the displacements along the x axis with the manubrium unclamped, and the annular ligament clamped. The slice spacing is 2 and the nominal number of elements per diameter is 35. The minimum x displacement is -44 nm and the maximum x displacement is 2208 nm.

Chapter 8

CONCLUSION AND FUTURE WORK

8.1 Summary

A preliminary model of the middle ear of the moustached bat was developed. Two MRM sets were used to create 3D-visualisation models and one set was used to create the final finite-element model. In addition, a set of histological serial sections was digitised in order to discern the fine details of soft tissues like the tympanic membrane, ligaments and muscles.

A programme for data reduction was written. It reduces the number of nodes of contours by eliminating those nodes which are redundant. The programme evaluates the position of the nodes and eliminates those which lie on a straight line.

A function was written which calculates the positions of the external loads representing the annular ligament. It searches for the boundary nodes of a given structure and returns a list of normalised vectors representing the external loads. This function was implemented in Fad, the finite-element data-manipulation programme.

Simulations were carried out in order to investigate convergence, sensitivity to tympanic-membrane shape, and to evaluate the effects of pressure and radial loads.

8.2 Conclusion

Through creating the model it was possible to evaluate the way open contours handle the connections between structures. The process has led to proposals for adjusting user-interaction with the programme and improved the way inter-structural connections are set up. For example, the setup of connections between structures has been improved and the programme now visualises the *xz* and *yz* planes which makes it easier to orient and smooth contours.

The part of the model representing the tympanic membrane was tested for convergence and the value for the nominal number of elements per diameter was set at 35. The convergence test was carried out with mesh resolutions varying from 10 to 75 elements per diameter. It showed a rise to a plateau level which continued from 30 to 45 elements per diameter and then started to slowly decrease in magnitude, i.e., as the size of the elements decreased, the maximum displacements decreased. This is a problem which needs to be explored further. Possible causes may be the lack of smoothness of the model or numerical instability due to the changing shape of the elements.

The tympanic membrane shows distortions caused by the preparation of the specimen for the MRM scan. A spline-interpolation technique was used to obtain a better representation of the shape of the membrane. There are other approaches available to approximate the shape of the tympanic membrane. The most accurate one is the use of moiré data. The moiré data are obtained using a phase-shift technique (Funnell & Decraemer, 1996) in which the pixel values are directly related to the *z* coordinate. Unfortunately, there is no moiré data available yet for the moustached bat. Another technique is the circular-arc interpolation proposed by Funnell (1975) and further described by Funnell (1996), which does not take any information about the shape of the tympanic membrane from the MRM data and relies purely on the boundary nodes of the membrane and the manubrium.

The spline-interpolation method was chosen because this technique has the advantage that a realistic shape of the membrane can be better specified using control points. Some of the curvature of the tympanic membrane is present and clearly does not entirely originate from distortion due to the preparation of the middle ear.

More time could be spent smoothing the model because the problems might lie with the boundaries of the tympanic membrane and the manubrium which are not completely smooth and accurate.

8.3 Future work

The values used here for the different parameters are estimates based on previously developed models. This is due to the fact that no experimental data are yet available for the bat. Efforts should be directed towards obtaining more experimental data. Dr. Henson is currently investigating the behaviour of the bat tympanic membrane when the smooth muscle is made to contract using drugs. It would also be valuable to obtain moiré data in order to model the tympanic membrane in a more realistic manner

More effort could be made to (semi-) automate the segmentation process, and different parts of the current system could be integrated into a more user-friendly environment. For example, real-time interaction between Fie and a 3D-viewer has the potential to create a more productive setup and simplified segmentation.

At present solid structures are modelled using shell-elements generated by the surface triangulation programme Tr3. This representation does not effectively characterize solid structures. To model the behaviour of solid structures in a more realistic way volume meshes need to be created, even though they are more complex to generate and lead to more computationally expensive simulations.

In some species (Decraemer et al. 2000) the malleus and incus do not move as a rigid body. To model this behaviour the incus and malleus need to be separated. This requires a closer look at the histology to obtain more information about the malleoincudal articular surfaces.

The present model neglects inertial and damping effects by assuming a low-frequency input. The bat's hearing system is more sensitive for higher frequencies. It would be of interest to run simulations for higher frequencies with the goal of obtaining more information about this aspect of the system's behaviour. This initiative would require more information about the structure and would expand the complexity of the model drastically because the damping and inertia of the system have to be taken into account.

Several researchers have assumed tension in the tympanic membrane (Rabbitt et al. 1986; Fay et al., 1999). Experiments and modelling of the middle ear of the moustached bat will contribute to a better understanding of the role of this applied tension.

Research has been conducted on the use of the stapedial muscle reflex to improve the performance of hearing aids (Hodges et al., 1997). A possible future clinical application might be the use of the smooth-muscle system to increase the tension of the tympanic membrane in order to enhance the sensitivity of the hearing system. This might be of interest, for example, in the fine-tuning of hearing aids or multi-channel cochlear implants.

References

Abou Khalil S, Funnell WRJ, Van Wijhe RG, Decraemer WF & Dirckx JJJ (2000): "Finite-element modelling of the human eardrum and middle ear" 23rd Midwinter Res. Mtg., Assoc. Res. Otolaryngol., St. Petersburg Beach

Bast TH, Anson BJ (1949): "*The temporal bone and the ear*" Springfield

Bathe KJ, Wilson EL, Peterson FE (1973): "SAP IV. A structural analysis program for static and dynamic response of linear systems" Report No. EERC 73-11, University of California, Berkeley

Beer HJ, Bornitz M, Drescher J, Schmidt R, Hardtke HJ, Hofmann G, Vogel U, Zahnert T, Huttenbrink KB (1997): "Finite element modelling of the human eardrum and applications"; in K.B. Huttenbrink, "*Middle Ear Mechanics in Research and Otosurgery*" Proc. of the Int. Workshop on Middle Ear Mechanics, Dresden, University of Technology, 40-47

Bondy G (1907): "Beiträge zur vergleichenden Anatomie des Gehörorgans der Sauger (Tympanicum, Membrana Shrapnelli und Chordaverlauf)" Ergeb. Anat. Entwicklungsgesch., 35, 293-408

Brown BH, Smallwood RH, Barber DC, Lawford PV, Hose DR (1999): "*Medical physics and biomedical engineering*" Institute of Physics publishing, Bristol and Philadelphia

Cornsweet T (1970): "*Visual perception*" Academic, New York

Crane Jr. HL, Gibbs NE, Poole Jr. WG, Stockmeyer PK (1976): "Algorithm 508. Matrix bandwidth and profile reduction" ACM Trans. Math. Software 2, 375-377, Complete source in "*Collected Algorithms*" from ACM.

Curry III TS, Dowdey JE, Murry Jr. RC (1990): "*Christensen's physics of diagnostic radiology*" Lea & Febiger, 432-505

Decraemer WF, Khanna SM, Funnell WRJ (1989): "Interferometric measurement of the amplitude and phase of tympanic membrane vibrations in cat" Hearing research, 38, 1-18

Decraemer WF, Khanna SM, Funnell WRJ (1991): "Malleus vibration mode changes with frequency" Hearing research, 54, 305-318

Decraemer WF, Khanna, SM, Funnell WRJ (2000): "Measurement and modelling of the three-dimensional vibration of the stapes in cat" Proc. Internat. Symp. on Recent Developments in Auditory Mechanics (Sendai, Japan, 1999 July), World Scientific Pub., US, UK, Singapore, 36-43

Fay JP, Puria S, Steele CR (1999): "Cat tympanic membrane: Annular plate and cone of strings model results in standing and travelling waves" 23rd Midwinter Res. Mtg., Assoc. Res. Otolaryngol., St. Petersburg Beach

Ferris P, Prendergast PJ, Rice HJ, Blayney AW (1998): "Finite element modelling of prostheses for ossicular chain reconstruction" Proc. Conference of the ESB, France

Funnell WRJ (1975): "*A theoretical study of eardrum vibrations using the finite-element method*" Ph.D. Thesis, McGill University, Montréal

Funnell WRJ, Laszlo CA (1978): "Modeling of the cat eardrum as a thin shell using the finite-element method" J. Acoust. Soc. Am., 63, 1461-1467

Funnell WRJ, Laszlo CA (1982): "A critical review of experimental observations on ear-drum structure and function" ORL, 44, 181-205

Funnell WRJ (1983): "On the undamped natural frequencies and mode shapes of a finite-element model of the cat eardrum" J.Acoust.Soc.Am., 73, 1657-1661

Funnell WRJ (1984a): "On the choice of a cost function for the reconstruction of surfaces by triangulation between contours" Comp. & Struct., 18, 23-26

Funnell WRJ (1984b): "On the calculation of surface areas of objects reconstructed from serial sections" J. Neurosci. Meth., 11, 205-210

Funnell WRJ, Decraemer WF, Khanna SM (1987): "On the damped frequency response of a finite-element model of the cat eardrum" J.Acoust.Soc.Am., 81, 1851-1859

Funnell WRJ, Khanna SM, Decraemer WF (1992): "On the degree of rigidity of the manubrium in a finite-element model of the cat eardrum" J. Acoust. Soc. Am., 91, 2082-2090

Funnell WRJ (1996a): "Finite-element modelling of the cat middle ear with elastically suspended malleus and incus" 19th Midwinter Res. Mtg., Assoc. Res. Otolaryngol., St. Petersburg Beach

Funnell WRJ (1996b): "Low-frequency coupling between eardrum and manubrium in a finite-element model" J. Acoust. Soc. Am., 99, 3036-3043

Funnell WRJ, Decraemer WF (1996): "On the incorporation of moiré shape measurements in finite-element models of the cat eardrum" J. Acoust. Soc. Am., 100, 925-932

Funnell WRJ, Decraemer WF, Von Unge M, & Dirckx JJJ (1999): "Finite-element modelling of the gerbil eardrum and middle ear" 23rd Midwinter Res. Mtg., Assoc. Res. Otolaryngol., St. Petersburg Beach

Fung YC (1993): "Biomechanics, mechanical properties of living tissues" Springer-Verlag, 466-499

Gonzalez RC, Woods RE (1993): "*Digital Image Processing*" Addison Wesley, 413-478

Guinan JJ, Peake WT (1967): "Middle-ear characteristics of anesthetized cats" J. Acoust. Soc. Am., 41, 1237-1261

Guyton AC (1991): "*Textbook of medical physiology, Eight edition*" W.B. Saunders Company

Ham AW (1969): "*Histology*" J.B. Lippincott Company

Helmholtz HLF (1869): "The mechanism of the middle–ear ossicles and of the eardrum" Plfügers Archiv. f. Physiol., Bonn,1, 1-60, (German). Translated by Buck AH and Smith N, Wood W, New York, 69 pp., 1873 and by Hinton J, Publ. New Sydenham Soc. London, 62, 97-155, 1874

Henson OW Jr. (1961): "Some morphological and functional aspects of certain structures of the middle ear in bats and insectivors" University of Kansas Science Bulletin, XLII, No.3, 151-255

Henson OW Jr. (1970): "The ear and audition"; in W.A. Wimstadt, "*Biology of bats*" Vol. 2, Academic Press, 181-256

Henson OW Jr., Henson MM (1972): "Middle ear muscle contractions and their relation to pulse- and echo-evoked potentials in the bat." Animal orientation and navigation , S.R. Galler et al., eds, 355-363. NASA Press, Washington, D.C.

Henson OW Jr., Henson MM (2000): "The tympanic membrane: highly developed smooth muscle arrays in the annulus fibrosus of mustached bats" JARO, 1, 25-32

Henson MM, Rask-Andersen H, Madden VJ Henson OW (2001a): "The human tympanic membrane: Smooth muscle in the region of the annulus fibrosus" ARO MidWinter Meeting, St. Petersburg Beach (in press)

Henson OW, Henson MM, Cannon J (2001b): "Comparative study of smooth muscle and collagen fibers in the attachment zone of the tympanic membrane" ARO MidWinter Meeting, St. Petersburg Beach (in press)

Herrera D, Maysinger D, Funnell WRJ, Cuello AC (1991): "Quantification of c-fos and GFAP expression following topical application of KCl to the brain surface" 3rd IBRO World Cong. Neuroscience, Montréal

Herrera DG, Maysinger D, Almazan G, Funnell WRJ, Cuello AC (1997): "Quantification of CFOS and glial fibrillary acidic protein in (GFAP) expression following topical application of potassium chloride to the brain surface" Brain Res., 784, 71-81

Hodges AV, Balkany J, Ruth RA, Lambert PR, Dolan-Ash S, Schloffman JJ (1997): "Electrical middle ear muscle reflex: use in cochlear implant programming" Otolaryncol. Head Neck Surg., 117, 255-261

Hyrtle J (1845): "Vergleichend-anatomische Untersuchungen über das innere Gehörorgan de Menschen und Säugetiere" Friedrich Ehrlich, Prag.

Kass M, Witkin, Terzopoulos D (1987): "Snakes: Active contour models" International journal of computer vision, 1, 321-331

Khanna SM, Tonndorf J (1972): "Tympanic membrane vibrations in cats studied by time-averaged holography" J. Acoust. Soc. Am., 51, 6, 1904-1920

Lord RM, Abel EW, Mills RP (1999): "A Finite Element Model of the Middle Ear" Proceedings of NAFEMS world congress '99 on Effective Engineering Analysis, 1, 487-494

MacDonald D (1995): "Display-Program for Display and segmentation of surfaces and volumes"

Marr D, Hildreth E (1980): "Theory of edge detection" Proc. R. Soc. London., B207, 187-217

Murphy RA, Herlihy JT, Megerman J (1974): "Force-generating capacity and contractile protein content of arterial smooth muscle" J. Gen. Physiol., 64, 691-705

Nigg BM, Herzog W (1999): "*Biomechanics of the musculo-skeletal system 2nd edition*" Wiley 1999

Novick A, Vaisnys JR (1964): "Echolocation of flying insects by the bat, Chilonycteris parnellii. Biol. Bulletin, 127, 478-488

Novick A (1977): "Acoustic orientation"; in W.A. Wimstadt, "*Biology of bats*" Vol. 3, Academic Press, 74-273

Onchi, Y (1961): "Mechanism of the middle ear" J. Acoust. Soc. Am., 33, 794-805

Özkaya, N, Nordin, M (1991): "*Fundamentals of Biomechanics: Equilibrium, motion, and deformation*" Van Nostrand Reinhold, New York

Rabbitt RD, Holmes MH (1986): "A fibrous dynamic continuum model of the tympanic membrane" J Acoust Soc Am, 80, 1716-1728

Relkin EM (1988): "Introduction to the analysis of middle ear function" in "*Physiology of the ear*" ed. Jahn AF and Santos-Sacchi J, Raven Press, New York, 103-123

Shaw EAG, Stinson MR (1981): "Network concepts and energy flow in the human middle-ear" J. Acoust. Soc. Am., 69, S43

Staněk VJ (1933): "*K topografické a srovnávací anatomii sluchového orgánu našich Chiropter*" Nákladem České Akademie Věd a Uměni, Prague

Stakgold I (1968): "Boundary value problems of mathematical physics" Vol.II., Macmillan, New York, 332-335

Stuhlman O Jr. (1937): "The nonlinear transmission characteristics of the auditory ossicles" J. Acoust. Soc. Am., 9, 119-128

Tepaske ER (1964): "Some morphological aspects and taxonomic relationships of the middle ear of bats" Ph.D. Thesis, Oklahoma State Univeristy

Von Békésy G (1960): "*Experiments in Hearing*" New York: McGraw-Hill

Wada H, Metoki T, Kobayashi T (1992): "Analysis of dynamic behavior of human middle ear using a finite-element method" J. Acoust. Soc. Am., 96, 3157-3168

Wassif K (1948): "Studies on the structure of the auditory ossicles and tympanic bone in Egyptian Insectivora, Chiroptera and Rodentia" Bull. Fac. Sci., Cario University, 27, 177-213

Wever EG, Lawrence M (1954): "*Physiological Acoustics*" Princeton University Press, Princeton, New Jersey, 1954

Wever EG and Vernon JA (1961): "The protective mechanisms of the bat's ear" Ann. Otol., Rhinol., & Laryngol., 70, 1-13

Williams KR, Blayney AW, Rice HJ (1997): "Middle ear mechanics as examined by the finite element method" Proc. of the Int. Workshop on Middle Ear Mechanics in Research and Otosurgery, Dresden, Germany, Editor Huttenbrink K, 67-75

Wilson JP, Bruns V (1983): "Middle-ear mechanics in the CF-bat Rhinolophus ferrumequinum" Hearing research, 10, 1-13

Yu X, Yla-Jaaski J (1995): "Interactive surface segmentation for medical images" Proceedings of SPIE, The International Society for Optical Engineering, Society of Photo-Optical Instrumentation Engineers, Bellingham, 519-527

Zhou X, Peck TL, Litchfield JB (1995): "Magnetic Resonance Microscopy" Annual reports on NMR spectroscopy, vol. 31, 31-80

Zwislocki, J (1962): "Analysis of the middle ear function, Part I Input impedance" J. Acoust. Soc. Am., 34, 1514-1523

Appendix 1

TR3 HEADER

This is the complete header of the Tr3 file produced by the Fie programme. The syntax is explained in section 5.4.5.

```
; RGVW 2000 09 11 New data file for dataset 16963
; Bat: Pteronotus parnellii rubiginosa
; voxel elements approx. 25 um
;
CONTOUR_NAMES
1:    -o OP -c 6 -r 150 1 -m 1 75.u  manubrium lateral 127
2:    -o OP -c 7 -r 150 1 -m 2 100.u -s s 1 -f f 1 manubrium medial 134 1
3:    -o CL -c 7 -r 150 1 -m 2 100.u manubrium medial 134 2
4:    -o OP -c 7 -r 150 1 -m 2 100.u -s f 5 -f s 1 manubrium medial 127 1
5:    -o OP -c 7 -r 150 1 -m 2 100.u -s f 1 manubrium medial 127 2
6:    -o OP -c 2 -r 150 1 -m 4 25.u   tm inferior 160
7:    -o OP -c 3 -r 150 1 -m 4 25.u   -f s 1 tm anterior 127
8:    -o OP -c 4 -r 150 1 -m 4 25.u   -s f 1 tm posterior 127
9:    -o OP -c 8 -r 150 1 -m 4 25.u   tm superior 119
10:   -o CL -c 4 -r 150 1 -m 2 150.u malleus 124
11:   -o OP -c 4 -r 150 1 -m 2 150.u -s f 12 -f s 12 malleus 120 1
12:   -o OP -c 4 -r 150 1 -m 2 150.u malleus 120 2
13:   -o OP -c 7 -r 150 1 -m 2 50.u  -s s 82 -f s 16 stapes crus anterior interior 109
14:   -o OP -c 7 -r 150 1 -m 2 50.u  -s f 88 -f s 1 stapes crus posterior exterior 113
15:   -o OP -c 7 -r 150 1 -m 2 50.u  stapes head 111
16:   -o OP -c 7 -r 150 1 -m 2 50.u  -f s 25 stapes head interior 109
17:   -o CL -c 7 -r 150 1 -m 2 100.u malleus/incus 80
18:   -o OP -c 7 -r 150 1 -m 2 100.u -s s 27 -f f 27 malleus/incus 87 1
19:   -o CL -c 7 -r 150 1 -m 2 100.u malleus/incus 95
20:   -o OP -c 7 -r 150 1 -m 2 100.u -s s 92 -f f 93 malleus/incus 118
21:   -o OP -c 7 -r 150 1 -m 2 100.u free
22:   -o OP -c 7 -r 150 1 -m 2 100.u -s f 24 -f s 23 malleus/incus 103 1
23:   -o OP -c 7 -r 150 1 -m 2 100.u malleus/incus 103 2
24:   -o OP -c 7 -r 150 1 -m 2 100.u -s f 23 malleus/incus 103 3
25:   -o OP -c 7 -r 150 1 -m 2 50.u  stapes head 108
26:   -o OP -c 7 -r 150 1 -m 2 100.u -s f 27 -f s 27 malleus/incus 87 2
27:   -o OP -c 7 -r 150 1 -m 2 100.u malleus/incus 87 3
28:   -o OP -c 7 -r 150 1 -m 2 50.u  -s f 14 stapes footplate 113
29:   -o OP -c 7 -r 150 1 -m 2 50.u  stapes footplate 111
30:   -o OP -c 3 -r 150 1 -m 2 100.u -s s 1 manubrium medial 133 1
31:   -o OP -c 3 -r 150 1 -m 2 100.u -s f 1 -f f 30 manubrium medial 133 2
32:   -o OP -c 3 -r 150 1 -m 2 100.u -s f 30 -f s 1 manubrium medial 133 3
33:   -o OP -c 7 -r 150 1 -m 2 50.u  stapes footplate 116
34:   -o OP -c 7 -r 150 1 -m 2 150.u -s s 93 -f f 92 malleus/incus 118
35:   -o OP -c 7 -r 150 1 -m 2 50.u  -s f 60 malleus/incus 113 1
36:   -o OP -c 7 -r 150 1 -m 2 50.u  -f s 38 malleus/incus 111 1
37:   -o OP -c 7 -r 150 1 -m 2 50.u  -s f 38 -f s 49 malleus/incus 111 2
38:   -o OP -c 7 -r 150 1 -m 2 50.u  malleus/incus 111 3
39:   -o OP -c 7 -r 150 1 -m 2 50.u  -f s 50 malleus/incus 108 1
40:   -o CL -c 7 -r 150 1 -m 2 50.u  stapes 103
41:   -o OP -c 2 -r 150 1 -m 1 50.u  -s f 92 tensor tympani 118 1
42:   -o OP -c 2 -r 150 1 -m 1 50.u  -s s 92 tensor tympani 118 2
43:   -o OP -c 2 -r 150 1 -m 1 50.u  tensor tympani 107
44:   -o OP -c 2 -r 150 1 -m 1 50.u  tensor tympani 120
45:   -o OP -c 2 -r 150 1 -m 2 100.u -b C -s s 43 -f f 43 tensor tympani on bone 107
46:   -o OP -c 2 -r 150 1 -m 2 100.u -b C -s s 44 -f f 44 tensor tympani on bone tail 120
47:   -o OP -c 2 -r 150 1 -m 2 100.u -b C -s f 42 -f f 41 tensor tympani on bone centre 118
48:   -o OP -c 7 -r 150 1 -m 2 150.u -s f 35 -f f 61 malleus/incus 113 2
49:   -o OP -c 7 -r 150 1 -m 2 150.u malleus/incus 111 3
50:   -o OP -c 7 -r 150 1 -m 2 150.u malleus/incus 108 2
51:   -o OP -c 7 -r 150 1 -m 2 150.u -s s 52 -f f 53 malleus 100 1
52:   -o OP -c 7 -r 150 1 -m 2 150.u -f s 53 malleus 100 2
53:   -o OP -c 7 -r 150 1 -m 2 100.u malleus 100 3
54:   -o OP -c 7 -r 150 1 -m 2 100.u malleus 134 1
55:   -o OP -c 7 -r 150 1 -m 2 100.u malleus 134 2
56:   -o OP -c 2 -r 150 1 -m 2 100.u -b C -s f 57 -f s 57 temporal bone lateral 108
57:   -o OP -c 2 -r 150 1 -m 2 100.u -s s 39 -f f 50 temporal bone con. to malleus 108
58:   -o OP -c 2 -r 150 1 -m 2 100.u -b C -s f 59 -f s 59 temporal bone lateral 111
59:   -o OP -c 2 -r 150 1 -m 2 100.u -s s 36 -f f 49 temporal bone con. to malleus 111
60:   -o OP -c 2 -r 150 1 -m 2 100.u -b C -s f 61 -f s 61 temporal bone lateral 113
61:   -o OP -c 2 -r 150 1 -m 2 100.u tempoal bone con. to malleus 113
62:   -o CL -c 2 -r 150 1 -m 1 50.u  stapedius muscle
63:   -o OP -c 2 -r 150 1 -m 1 50.u  -s f 67 -f s 64 stapedius muscle 108 1
64:   -o OP -c 2 -r 150 1 -m 1 50.u  -f s 65 stapedius muscle 108 2
```

```
65:  -o OP -c 7 -r 150 1 -m 2 50.u  stapedius muscle con stapes 108 3
66:  -o OP -c 2 -r 150 1 -m 1 50.u  -f s 67 stapedius muscle 108 4
67:  -o OP -c 1 -r 150 1 -m 1 50.u  -b C stapedius muscle 108 5
68:  -o CL -c 2 -r 150 1 -m 1 50.u  stapedius muscle 111
69:  -o OP -c 4 -r 150 1 -m 2 100.u free
70:  -o OP -c 7 -r 150 1 -m 2 50.u  -s s 15 -f f 29 stapes crus anterior exterior 111
71:  -o OP -c 2 -r 150 1 -m 2 6.    -b C -s f 93 -f s 93 temporal bone lateral 118
72:  -o CL -c 2 -r 150 1 -m 2 6.    -b C temporal bone lateral 120
73:  -o OP -c 3 -r 150 1 -m 2 50.u  -s f 74 -f s 75 incudalstapedial joint 107 1
74:  -o OP -c 4 -r 150 1 -m 2 50.u  -s s 76 -f s 75 incudostapedial joint 107 2
75:  -o OP -c 5 -r 150 1 -m 2 50.u  -f f 76 incudostapedial joint 107 3
76:  -o OP -c 6 -r 150 1 -m 2 50.u  incudostapedial joint 107 4
77:  -o OP -c 4 -r 150 1 -m 2 50.u  -s s 133 -f f 25 icudostapedial joint 108 1
78:  -o OP -c 5 -r 150 1 -m 2 50.u  -s f 65 stapes crus posterior exterior 108
79:  -o OP -c 7 -r 150 1 -m 2 50.u  stapes footplate 106
80:  -o OP -c 7 -r 150 1 -m 2 50.u  -s f 69 stapes footplate 109
81:  -o OP -c 7 -r 150 1 -m 2 50.u  -f f 79 stapes footplate interior 107
82:  -o OP -c 7 -r 150 1 -m 2 50.u  -f f 80 stapes footplate interior 109
83:  -o OP -c 7 -r 150 1 -m 2 50.u  -f s 29 stapes footplate interior 111
84:  -o OP -c 7 -r 150 1 -m 2 50.u  -s s 83 -f s 88 stapes crus posterior interior 111
85:  -o OP -c 7 -r 150 1 -m 2 50.u  -s f 28 -f s 86 stapes crus posterior single 113
86:  -o OP -c 7 -r 150 1 -m 2 50.u  stapes crus interior all 113
87:  -o OP -c 7 -r 150 1 -m 2 50.u  -s f 86 -f s 88 stapes footplate interior 113
88:  -o OP -c 7 -r 150 1 -m 2 50.u  -s f 16 stapes crus anterior interior 113
89:  -o OP -c 7 -r 150 1 -m 2 50.u  -s f 15 stapes head 111
90:  -o OP -c 7 -r 150 1 -m 2 50.u  -s f 84 -f f 89 stapes head interior 111
91:  -o OP -c 7 -r 150 1 -m 2 50.u  -s s 81 -f s 79 stapes footplate/crus 108
92:  -o OP -c 7 -r 150 1 -m 2 150.u tensor tympani connection 119
93:  -o OP -c 7 -r 150 1 -m 2 6.    -b C tensor tympani connection on bone 118
94:  -o CL -c 1 -r 150 1 -m 2 6.    -b C temporal bone lateral 103
95:  -o OP -c 7 -r 150 1 -m 2 50.u  -s s 33 -f f 33 stapes footplate interior 116
96:  -o OP -c 7 -r 150 1 -m 2 50.u  -s f 78 -f s 25 stapes head interior 108
97:  -o OP -c 3 -r 150 1 -m 2 50.u  -s f 133 -f s 98 stapes crus exterior 109
98:  -o OP -c 7 -r 150 1 -m 2 50.u  -f s 80 stapes crus exterior b
99:  -o OP -c 6 -r 1 1 stapes footplate spring 1a
100: -o OP -c 6 -r 1 1 stapes footplate spring 2a
101: -o OP -c 6 -r 1 1 -b C stapes footplate spring 1b fixed end
102: -o OP -c 6 -r 1 1 -b C stapes footplate spring 2b fixed end
103: -o OP -c 6 -r 1 1 stapes footplate spring 3a
104: -o OP -c 6 -r 1 1 -b C stapes footplate spring 3b fixed end
105: -o OP -c 6 -r 1 1 stapes footplate spring 4a
106: -o OP -c 6 -r 1 1 -b C stapes footplate spring 4b fixed end
107: -o OP -c 2 -r 150 1 -m 1 50.u  -s s 109 -f f 9 an lig anterior 9 1
108: -o OP -c 3 -r 150 1 -m 1 50.u  -s f 109 -f f 9 an lig anterior 9 2
109: -o OP -c 1 -r 150 1 -m 2 100.u -b C an lig anterior on bone 9
110: -o OP -c 2 -r 150 1 -m 1 50.u  -s s 112 -f s 9 an lig posterior 9 1
111: -o OP -c 3 -r 150 1 -m 1 50.u  -s f 112 -f s 9 an lig posterior 9 2
112: -o OP -c 1 -r 150 1 -m 2 100.u -b C an lig posterior on bone 9
113: -o OP -c 2 -r 150 1 -m 1 50.u  -s s 115 -f f 8 an lig anterior 8 1
114: -o OP -c 3 -r 150 1 -m 1 50.u  -s f 115 -f f 8 an lig anterior 8 2
115: -o OP -c 1 -r 150 1 -m 2 100.u -b C an lig anterior on bone 8
116: -o OP -c 2 -r 150 1 -m 1 50.u  -s s 118 -f s 7 an lig posterior 7 1
117: -o OP -c 3 -r 150 1 -m 1 50.u  -s f 118 -f s 7 an lig posterior 7 2
118: -o OP -c 1 -r 150 1 -m 2 100.u -b C an lig posterior on bone 7
119: -o OP -c 2 -r 150 1 -m 1 50.u  -s s 121 -f f 6 an lig anterior 6 1
120: -o OP -c 3 -r 150 1 -m 1 50.u  -s f 121 -f f 6 an lig anterior 6 2
121: -o OP -c 1 -r 150 1 -m 2 100.u -b C an lig anterior on bone 6
122: -o OP -c 2 -r 150 1 -m 1 50.u  -s s 124 -f s 6 an lig posterior 6 1
123: -o OP -c 3 -r 150 1 -m 1 50.u  -s f 124 -f s 6 an lig posterior 6 2
124: -o OP -c 1 -r 150 1 -m 2 100.u -b C an lig posterior on bone 6
125: -o OP -c 4 -r 150 1 -m 1 50.u  -s s 127 -f s 9 an lig centre 1
126: -o OP -c 3 -r 150 1 -m 1 50.u  -s f 127 -f f 9 an lig centre 1 2
127: -o OP -c 1 -r 150 1 -m 2 100.u -b C an lig centre on bone
128: -o OP -c 4 -r 150 1 -m 1 50.u  -s s 130 -f f 129 an lig centre 1
129: -o OP -c 3 -r 150 1 -m 1 50.u  -s f 130 an lig centre 1 2
130: -o OP -c 1 -r 150 1 -m 2 100.u -b C an lig centre on bone
131: -o OP -c 2 -r 150 1 -m 1 50.u  -s f 135 -f s 132 stapedius muscle 109
132: -o OP -c 2 -r 150 1 -m 1 50.u  stapedius muscle 109 2
133: -o OP -c 1 -r 150 1 -m 1 50.u  -f s 134 stapedius muscle con stapes 109 3
134: -o OP -c 2 -r 150 1 -m 1 50.u  -f s 135 stapedius muscle 109 4
135: -o OP -c 1 -r 150 1 -m 1 50.u  -b C stapedius muscle 109 5
0
CAP
 TAIL 1 -2
 TAIL 3
 HEAD 62
 TAIL 68
 TAIL 95 -33
 HEAD 43 -45
 TAIL 44 -46
 HEAD 43 -45
 HEAD 26 27
 HEAD 17
 TAIL 71 93
 HEAD 79 -81 91
 HEAD 97 98 13
 TAIL 14 28 85 87 88
 HEAD 94
 HEAD 74 75 -76
 HEAD 96 65 78
```

```
 TAIL 128 -129 -130
 TAIL 127 126 -125
 TAIL 123 6 -120
 HEAD 112 111 -110
 HEAD 109 108 -107
 END
JOIN
 1: 7 1 8 to 6              ; tm
 2: 9 to 7 1 8              ; tm
 3: 10 to 1 5 4             ; manubrium
 4: 32 30 to 3              ; tm manubrium
 5: 31 -30 1 to -2 1        ; tm manubrium
 6: 17 to 18 -27            ; malleus/incus
 7: 26 18 to 19             ; malleus/incus
 8: 50 39 to 49 36 38 37    ; malleus/incus
 9: 36 38 37 49 to 35 48    ; malleus/incus
 10: 48 35 to 20 34                 ; malleus/incus
 11: 20 34 to 11 12                 ; malleus/incus
 12: 19 to 51 -53 -52       ; malleus/incus
 13: 5 4 1 to 31 32 1       ; malleus/incus
 14: 11 12 to 10            ; malleus/incus
 15: 24 22 23 to 39 50      ; malleus/incus
 16: 51 -53 -52 to 40 22 23 24 ; malleus/incus
 17: -42 92 41 -47 to 44 -46        ; malleus/incus
 18: 48 -61 35 to 20 -93 34 -92     ; malleus connection tensor tympani
 19: 20 -93 34 -92 to 12 11         ; malleus connection tensor tympani
 20: 40 to 73               ; stapes
 21: 89 -90 15 to 14 88     ; stapes
 22: -70 15 to 85           ; stapes
 23: 84 to -86              ; stapes
 24: -84 83 to 86 87        ; stapes
 25: -98 -97 -133 77 to -70 15 ; stapes
 26: -90 89 to 88 14        ; stapes
 27: -25 -16 -13 82 -80 -98 -97 -133 77 to 89 -90 -84 83 29 -70 15 ; stapes
 28: 87 to 33               ; stapes footplate
 29: 79 -81 91 to 80 -82 98         ; stapes footplate
 30: 80 to -29              ; stapes footplate
 31: 29 to 28               ; stapes footplate
 32: 28 to -33              ; stapes footplate
 33: -82 13 16 to -83 84 90         ; stapes footplate
 34: 62 to 67 63 64 65 66  ; stapedius muscle
 35: 135 131 132 133 134 to 68 ; stapedius muscle
 36: 67 63 64 65 66 to 135 131 132 133 134          ; stapedius muscle
 37: 40 to 73                               ; incudalstapedial joint
 38: 74 73 75 -76 to -65 77 -25 -96 -78             ; incudalstapedial joint
 39: -25 -96 -78 -65 77 to -25 -16 -97 -133 77      ; incudalstapedial joint
 40: 43 -45 to -42 92 41 -47        ; tensor tympani
END
MERGE
99 28 2. ; spring to stapes
100 28 2.         ; spring to stapes
103 79 2.         ; spring to stapes
105 33 2.         ; spring to stapes
 0
SPRINGS
99 101 D 1.
100 102 D 1.
103 104 D 1.
105 106 D 1.
 0
MATERIALS
1 20.M 0.3 1000. ;strong connective tissue (N/m2, kg/m3)
2 200.M 0.3 1900.;bone
3 2.M 0.3 1000.   ;soft connective tissue
4 20.M 0.3 1000. ;strong connective tissue tympanic membran
 0
```